Nanoscale

ROYAL SOCIETY OF CHEMISTRY

MINIREVIEW

View Article Online
View Journal | View Issue

Cite this: *Nanoscale*, 2020, **12**, 17982

Nanostructured manganese dioxide for anticancer applications: preparation, diagnosis, and therapy†

Zheng Zhang and Yuanhui Ji *

Nanostructured manganese dioxide (MnO_2) has attracted extensive attention in the field of anticancer applications. As we all know, the tumor microenvironment is usually characterized by a high glutathione (GSH) concentration, overproduced hydrogen peroxide (H_2O_2), acidity, and hypoxia, which affect the efficacy of many traditional treatments such as chemotherapy, radiotherapy, and surgery. Fortunately, as one kind of redox-active nanomaterial, nanostructured MnO_2 has many excellent properties such as strong oxidation ability, excellent catalytic activity, and good biodegradability. It can be used effectively in diagnosis and treatment when it reacts with some harmful substances in the tumor site. It can not only enhance the therapeutic effect but also adjust the tumor microenvironment. Therefore, it is necessary to present the recent achievements and progression of nanostructured MnO_2 for anticancer applications, including preparation methods, diagnosis, and treatment. Special attention was paid to photodynamic therapy (PDT), bioimaging and cancer diagnosis (BCD), and drug delivery systems (DDS). This review is expected to provide helpful guidance on further research of nanostructured MnO_2 for anticancer applications.

Received 27th May 2020,
Accepted 30th July 2020

DOI: 10.1039/d0nr04067c

rsc.li/nanoscale

1. Introduction

Cancer is one of the high-mortality diseases due to the lack of effective therapies. However, there are many promising strategies for cancer diagnosis and therapy with the rapid development of nanotechnology and materials science. Many anticancer strategies rely on advanced nanomaterials, such as 2D

Jiangsu Province Hi-Tech Key Laboratory for Biomedical Research, School of Chemistry and Chemical Engineering, Southeast University, Nanjing, 211189, People's Republic of China. E-mail: yuanhui.ji@seu.edu.cn, yuanhuijinj@163.com

†Electronic supplementary information (ESI) available. See DOI: 10.1039/d0nr04067c

Zheng Zhang

Zheng Zhang received his master's degree from Zhengzhou University in 2018. He is currently a Ph.D. candidate in the school of chemistry and chemical engineering of Southeast University. His research interests focus on controlled drug release systems and nanomaterials for anticancer applications.

Yuanhui Ji

Yuanhui Ji received her bachelor's degree and Ph.D. in Chemical Engineering from Nanjing Tech University in 2004 and 2010, respectively. After that, she worked as a postdoctoral research fellow at the Luleå University of Technology (2010–2011). She worked as an Alexander von Humboldt Research Fellow at Technische Universität Dortmund in Germany (2012–2016). She has been a professor at Southeast University in China since 2016. Her research interests mainly focus on controlled drug delivery systems, modeling analysis of drug release kinetics and drug crystallization, as well as nanomaterials and nanomedicine for anticancer applications.

nanosheets,[1,2] polyoxometalates,[3,4] and metallic complex nanoparticles.[5,6] Similarly, nanostructured manganese dioxide (MnO_2) has also become a favoured material for anticancer applications in recent years. MnO_2 is one of the common minerals, which exhibits many unique chemical and physical properties.[7,8] As has been reported, the well-known applications of MnO_2 are in the fields of catalysts,[9,10] oxidants,[11] ferrite,[12–14] achromatic agents,[15] energy storage,[16,17] *etc*. The extensive applications are ascribed to its excellent properties, such as non-stoichiometric composition, rich polymorphism, and structural variety.[18–20] MnO_2 nanomaterials have similar structural characteristics as revealed by abundant research studies. The MnO_2 framework is constituted by an edge- or corner-sharing [MnO_6] octahedral unit, and shows structural flexibility and diverse forms such as α-, β-, γ-, and δ-MnO_2.[7,8,21] In recent years, nanostructured MnO_2 has opened up a new field in biomedical materials;[22–24] afterward, it has been becoming more and more popular.[25,26] In particular, the published papers have been growing drastically in anticancer applications.[27–29] Researchers have also exhibited unprecedented enthusiasm and pushed it to a higher development stage.[30–32] To a great extent, the application of materials depends on its preparation technology. As a consequence, nanostructured MnO_2 also shows diversity due to the different preparation methods.[33] The major approaches and technologies of nanostructured MnO_2 in anticancer applications are summarized here, including the bio-mineralization method, template method, redox method, and some other methods.[34–36]

With the extensive studies, nanostructured MnO_2 has shown great prospects in anticancer applications[37] such as photodynamic therapy (PDT),[38,39] bioimaging and cancer diagnosis (BCD),[40,41] and drug delivery systems (DDS).[28,42] As we already know, the tumor microenvironment is an important influencing factor for many traditional cancer treatments, such as chemotherapy, radiotherapy, and surgery.[43–45] In this regard, the tumor microenvironment is usually characterized by high glutathione (GSH) concentration, overproduced hydrogen peroxide (H_2O_2), mildly acidic nature, and hypoxia.[46–49] As one kind of necessary substance in many physiological activities, the concentration of GSH is *ca.* 2–10 mM in tumor cells, which is at least four times higher than that in normal cells.[50] Notably, it is 100–1000-fold higher in the intracellular fluid than in the extracellular fluid.[51] Although the PDT has the advantages of precision, high efficiency, minimal damage, and less toxicity,[52,53] the high concentration of GSH has the characteristic of reactive oxygen species (ROS) consumption, which makes it an enemy of PDT and reduces the treatment effect.[54–57] To address this issue, it is necessary to reduce the level of GSH in the tumor site.[58,59] It is gratifying that nanostructured MnO_2 can enhance anticancer efficiency by reacting with GSH.[60] On the other hand, tumor cells are mildly acidic due to severe glycolysis.[61,62] Besides, tumor cells have the characteristics of infinite growth, proliferation, neovascularization, invasion, and metastasis, which are closely related to endogenous H_2O_2.[63] A large amount of endogenous H_2O_2 is produced and accumulated during normal cell carcinogenesis, which causes persistent oxidative stress and DNA oxidative damage.[64] Therefore, the tumor microenvironment is mildly acidic and H_2O_2-rich compared with normal cells.[40,65,66] In the as-described tumor microenvironment, MnO_2 can be used to achieve the enhancement effect by decomposing H_2O_2 into O_2.[67,68] It is promising to surmount hypoxia by utilizing tumor microenvironment-sensitive MnO_2.[69,70] Delightingly, the generated water-soluble Mn^{2+} ions have been used as a perfect magnetic resonance imaging (MRI) contrast agent[71,72] for the recognition and diagnosis of cancer. Besides, as an excellent nanomaterial with low toxicity,[73] strong adsorption, and good biocompatibility, nanostructured MnO_2 can carry many anticancer drug molecules and degrade under GSH/mildly acidic conditions.[74,75] Therefore, nanostructured MnO_2 could be used as a nanocarrier and/or "gatekeeper" for drug delivery.[76,77] Besides so many excellent properties, nanostructured MnO_2 also has made great progress in radiotherapy (RT), photothermal therapy (PTT), chemodynamic therapy (CDT), regulation of the tumor microenvironment (RTM), *etc*.[78–80] Therefore, it mostly uses the synergistic treatment form rather than a single treatment method, which not only increases the utilization rate but also improves the therapeutic effect.[81–83]

As a tumor microenvironment-sensitive and rather promising nanomaterial,[84–86] nanostructured MnO_2 has attracted extensive attention in the field of anticancer applications due to its excellent properties. It can be used effectively in diagnosis and treatment when it reacts with some harmful substances in the tumor site. Although the research time was short, it is still essential to summarize the recent achievements and progression of anticancer applications, including preparation methods, diagnosis, and therapy. As shown in Fig. 1, the progress of fabrication and anticancer applications will be

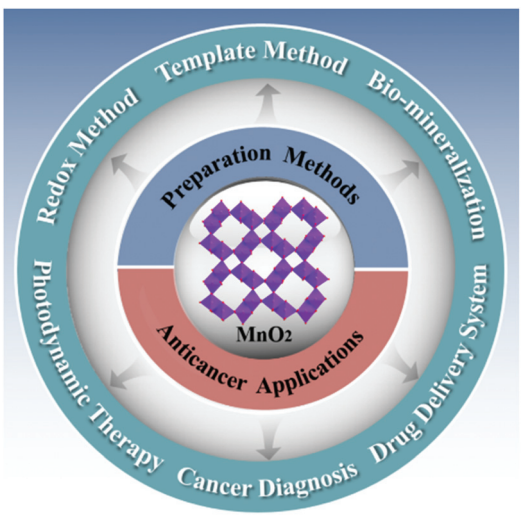

Fig. 1 Schematic illustration of nanostructured MnO_2 for anticancer applications, including preparation methods, photodynamic therapy (PDT), bioimaging and cancer diagnosis (BCD), and drug delivery systems (DDS).

systemically summarized, including PDT, BCD, DDS, and some other applications. A detailed summary has been listed in Table 1 (ESI†), including the type of MnO_2, various material applications, and advantages. Besides, future perspectives and challenges of nanostructured MnO_2 also will be discussed in detail. This review is expected to provide helpful guidance on nanostructured MnO_2 for anticancer applications.

2. Preparation methods of nanostructured MnO_2

The MnO_2 framework is usually constituted by an edge- or corner-sharing [MnO_6] octahedral unit as revealed by abundant research studies. Moreover, it shows structural diversity, such as nanosheet, nanoflower, nanowire, and nanoshell structures.[76,87,88] As a cheap and common transition metal oxide, there are many different preparation methods of nanostructured MnO_2.[20,74,89] Besides, different preparation methods lead to different sizes, shapes, structures, and applications.[90,91] In this section, we will summarize and introduce the representative methods which are frequently used in the field of anticancer applications, including the bio-mineralization method, template method, redox method, and some other methods.

2.1 Bio-mineralization method

With respect to the therapeutic nanoagents, the bio-mineralization method is a potential technology to combine biological macromolecules with inorganic materials.[92–94] More specifically, bio-mineralization refers to the process of preparing inorganic minerals through the regulation of biomacromolecules.[95,96] Unlike general mineralization, bio-mineralization technology involves the participation of bio-macromolecules and organic matrices.[97] In the process, bio-organic substances (such as serum albumin) would transform ions into solid minerals *via* the control or/and influence under physicochemical conditions.[98] They can control the shape and performance of inorganic materials as a nucleating agent, a synergetic regulator, or a template of mineral ions.[99] After bio-organic substances were introduced to direct the nucleation of Mn^{2+}, Mn^{2+} spontaneously formed MnO_2 *via* growth or oxidation in alkaline solutions. In anticancer applications, the frequently used bio-organic substances were plasma proteins such as bovine serum albumin (BSA), human serum albumin (HSA), and genetically engineered protein.[97,100]

As shown in Fig. 2a, Xiao *et al.*[101] provided a novel strategy to prepare polymer, BSA, and MnO_2 hybrid nanoparticles ($PMHN_S$) *via* the bio-mineralization method. A series of $PMHN_S$ were synthesized with the formation of MnO_2 nanoparticles in the albumin (BSA). Taking dopamine (DA) as an example, the PMHN-DA produced has a spherical structure with an average diameter of *ca.* 60 nm (Fig. 2c). In high resolution transmission electron microscopy (HRTEM) images (Fig. 2d), there were some black nanodots with diameters of *ca.* 2.5 ± 0.7 nm, which corresponded to the MnO_2 produced by bio-mineralization. The innovative study provided a strategy, which can help produce multifunctional and biocompatible nanotherapeutic agents. As we all know, HSA is one of the most abundant plasma proteins, which can also sequester inorganic ions under alkaline conditions.[102] For instance, Chen *et al.*[103] designed a multi-functional HSA-coated MnO_2 nanoparticle. In the process, the premodified HSA induced the formation of MnO_2 nanoclusters under alkaline conditions. Finally, the multi-component nanoparticles were obtained *via* bio-mineralization. Some genetically engineered proteins also

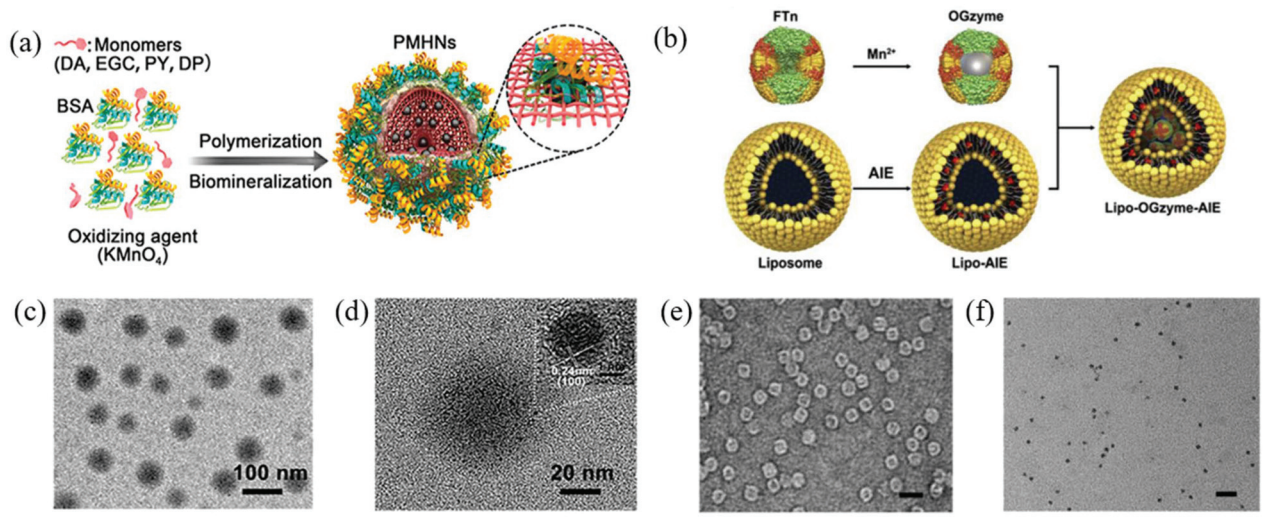

Fig. 2 (a) Schematic description of the preparation process of MnO_2 hybrid nanoparticles. Reproduced with permission from ref. 101. Copyright 2018 American Chemical Society. (b) Structures and preparation process of MnO_2 nanoparticles inside the FTn. Reproduced with permission from ref. 104. Copyright 2019 Elsevier Ltd. TEM (c) and HRTEM (d) images of the PMHN-DA nanoparticles. Reproduced with permission from ref. 101. Copyright 2018 American Chemical Society. TEM images of OGzymes (e) and the MnO_2 core (f); scale bar: 20 nm. Reproduced with permission from ref. 104. Copyright 2019 Elsevier Ltd.

can be used to prepare MnO_2 *via* the bio-mineralization method. In order to obtain a hypoxia-tropic nanozyme, Gao and co-workers[104] creatively prepared MnO_2 nanoparticles inside the hollow cavity of genetically engineered ferritin nanocages (FTn). In the bio-mineralization process, the FTn was used to capture metal ions and for future nucleation (Fig. 2b). The metal ions and O_2 (or H_2O_2) can diffuse through the channel structure of FTn protein. Moreover, there were a large number of metal ion-bonding residues at the interior ferroxidase centers, which made the hollow cavity interior a natural nucleation nanoreactor. Mn^{2+} was oxidized and nucleated into MnO_2 nanoparticles in the H_2O_2-containing alkaline solution. The TEM image showed that the FTn shell was a hollow structure with a diameter of *ca.* 12 nm (Fig. 2e). MnO_2 was a monodisperse spherical structure with a diameter of *ca.* 5 nm (Fig. 2f). After the calculation, it was found that there were ~160 Mn atoms per FTn.

For the anticancer applications of nanostructured MnO_2, the bio-mineralization method is one of the most effective methods due to the advantages of cost-effectiveness, convenience, and the environmentally benign nature.[105,106] The above pioneering studies have provided novel insights and helpful guidance for the design of the bio-mineralization method. For more detailed works, one could focus on several published papers.[107–109]

2.2 Template method

The template method is a general method, which can be used to prepare nanomaterials with various shapes.[110,111] Theoretically, the template can be any material with a nanostructure.[112] To our knowledge, the template method can be divided into the soft template method and hard template method according to the type of template.[113] As shown in Fig. 3a, the template method usually includes the following steps: (1) template preparation; (2) preparation of MnO_2 depending on the template; and (3) removal or non-removal of the templating agent as required.[114]

2.2.1 Soft template method. As a structure-oriented agent, soft templates include surfactants, flexible organic molecules, and block copolymers.[115,116] Micelles with different morphologies would be formed according to the concentration of surfactants. These micelle structures make inorganic materials show a specific distribution trend driven by the electrostatic interactions, hydrogen bonds and van der Waals force between surfactant molecules and nanomaterials. Remarkably, the soft templates can produce various MnO_2 structures (*e.g.*, nanosheets, nanospheres, and nanorods) by adjusting the precursors and reaction conditions.[23] Furthermore, the synthesis process of nanostructured MnO_2 usually involves organic–inorganic self-assembly. Based on these principles, He *et al.*[117] first achieved a honeycomb MnO_2 ($hMnO_2$) nanostructure as a new drug carrier for GSH-triggered drug release. To further extend its application, they[118] synthesized honeycomb MnO_2 ($hMnO_2$) nanocarriers by using oleic acid (OA) as both the template and reducing agent. In their design, $hMnO_2$ was prepared by the redox reaction of oleic acid (OA) and $KMnO_4$. The size of prepared $hMnO_2$ was *ca.* 136 nm. The preparation method was simple. Firstly, $KMnO_4$ was dissolved in water and fleetly stirred for *ca.* 0.5 h. Then, OA was added and the mixture was reacted for *ca.* 5 h. Afterwards, the product was centrifuged and washed to remove the residual reactant. The SEM (Fig. 3b) and TEM (Fig. 3c) images showed that the $hMnO_2$ nanocarriers has a honeycomb structure and consisted of some lamellar MnO_2 platelets. As an important preparation method, the soft template method has many advantages. Generally, there are various forms of the soft template, the preparation method is simple, the cost is low, and complex equipment is not needed. Therefore, this method is often used to prepare nanomaterials.

2.2.2 Hard template method. Although the soft template method is general, it still has limitations. Generally speaking,

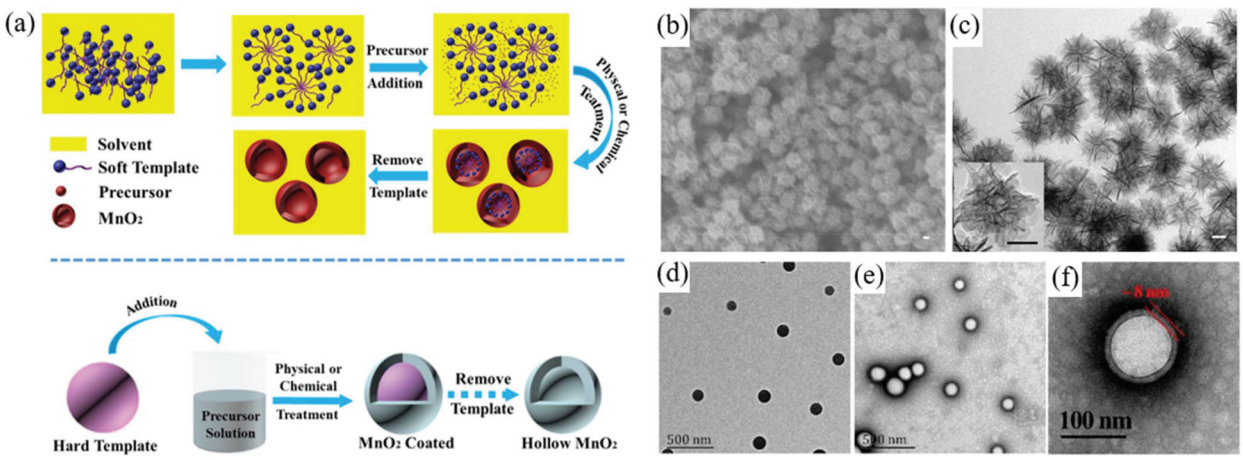

Fig. 3 (a) Schematic description of the templating process. SEM image (b) and TEM image (c) of $hMnO_2$ nanocarriers; scale bars: 40 nm. Reproduced with permission from ref. 118. Copyright 2017 WILEY-VCH Verlag GmbH & Co. KGaA, Weinheim. TEM image of PLGA (d) and $HMnO_2$ (e), and a magnified TEM image of $HMnO_2$ (f). Reproduced with permission from ref. 122. Copyright 2019 Elsevier B.V.

it is difficult to control the size, shape, and uniformity of products. The residual surfactants, organic compounds, and macromolecules may increase the resistance of ions.[23,113] Besides, the template-removal process is time-consuming.[23,112,113] As a comparison, the hard template method is a promising method to synthesize MnO_2 nanostructures. Hard templates are mainly rigid templates maintained by covalent bonds, such as polymers, porous silicon, metal templates, and carbon nanotubes.[119,120] Since no surfactant is involved, the interference is effectively reduced in the hard template method. Typically, Yang *et al.*[121] synthesized an intelligent hollow manganese dioxide (H-MnO_2) nanoplatform *via* the hard template method. In their work, monodisperse SiO_2 nanoparticles were prepared and selected as the hard template. After that, $KMnO_4$ was reduced by unreacted organosilica. Next, Na_2CO_3 solution was used to dissolve SiO_2 (H-MnO_2). Some polymers also can be selected to prepare MnO_2 as a hard template. Similarly, Wang *et al.*[122] synthesized platelet membrane functionalized bufalin-loaded $HMnO_2$ nanoparticles (PLTM-$HMnO_2$@Bu NPs). In their innovative preparation process, the poly(lactic-*co*-glycolic acid) (PLGA) nanoparticle (Fig. 3d) was selected as a hard template. The surface of PLGA nanoparticles has a lot of hydroxyl groups (–OH), which can react with $KMnO_4$. Therefore, the MnO_2 shell grew on the surface of PLGA nanoparticles. Finally, the PLGA cores were etched with acetone. The TEM image of hollow MnO_2 (Fig. 3e) clearly showed the hollow structure with an outer layer thickness of ~8 nm (Fig. 3f).

In summary, the template method has become the preferred method to prepare shell-like nanostructured MnO_2, and the soft template method has many advantages, such as simple operation, various forms, and easy construction.[23,112] However, it is difficult to control the size, shape, and uniformity.[23] The residual surfactants, organic compounds, and macromolecules not only increase the resistance of ions, but also the removal process is time-consuming. In contrast, there is no interference of the surfactant in the hard template method. Therefore, the removal process is avoided. Besides, the hard template has higher stability and can strictly control the size and morphology. However, the structure is relatively simple; so the morphology usually changes less. It is necessary to develop a preparation method which is simple, rapid, economical, and environment-friendly, and a lot of effort is still required to prepare unique MnO_2 nanostructures.

2.3 Redox method

For MnO_2 preparation, the redox method is another frequently used method due to its convenience and efficiency.[90,123] One of the redox methods is the Mn^{7+} ($KMnO_4$) reduction method. As a strong oxidant, $KMnO_4$ can be used to prepare MnO_2 by reacting it with some reducing agents.[80,124] It can be divided into inorganic reduction and organic reduction according to the type of reductant. Micromolecular organics, polymers, and proteins are frequently used organic compounds for reaction with $KMnO_4$. Besides, the other redox method is the Mn^{2+} ($MnCl_2$) oxidation method. The representative method was first proposed by Kai *et al.*[125] The method was widely used to prepare single-layer MnO_2 nanosheets for anticancer applications. According to the method, Mn^{2+} was oxidized with H_2O_2 in the presence of tetramethylammonium hydroxide (TMA·OH). The MnO_2 nanosheet can be directly obtained in a single step by chemical oxidation of Mn^{2+} ions.

2.3.1 Mn^{7+} ($KMnO_4$) reduction method

2.3.1.1 Inorganic reduction. For the Mn^{7+} ($KMnO_4$) reduction method, some inorganic reagents are often used to reduce $KMnO_4$, such as H_2O_2, $Na_2S_2O_3$, and $MnSO_4$.[38,126,127] For instance, Zhang *et al.*[128] prepared phase-change material based nanoparticles. In their innovative work, they first produced ultra-small MnO_2 (sMnO_2) nanosheets by using the reaction between $KMnO_4$ and H_2O_2. The TEM image (Fig. 4a) revealed that the uniform size of ultra-small sMnO_2 nanosheets was *ca.* 10 nm. Recently, Zhang *et al.*[129] designed an all-in-one nanoplatform for high efficiency therapy. In this novel design, g-C_3N_4 and DOX were encapsulated in ZIF-8, and then the nanoparticles were loaded with MnO_2 nanodots and modified with F127 (FMZ/DC, F127-MnO_2-ZIF@DOX/C_3N_4). MnO_2 nanodots were synthesized by the redox reaction between $MnSO_4$ and $KMnO_4$. TEM characterization was further conducted, and the uniformly dispersed MnO_2 nanodots (red arrows) were located on the surface of ZIF-8 (Fig. 4b). Similarly, Yang *et al.*[38] reported biomimetic hybrid nanozymes. In the preparation process, they used excess $Na_2S_2O_3$ to reduce $KMnO_4$. The size and zeta potential (Fig. 4c) of the prepared MnO_2 nanoparticles were 36 nm and −31.2 mV (pH 7.4), respectively. The inorganic reduction method was not only simple but also efficient. Therefore, this strategy was widely used to prepare nanostructured MnO_2.

2.3.1.2 Organic reduction. In addition to the inorganic reduction, organic reduction is another representative and promising method to produce nanostructured MnO_2 for anticancer applications.[87,130,131] Some organic compounds were used to react with $KMnO_4$, including micromolecular organics, polymers, proteins.[132–135] For micromolecular organics, Zhang *et al.*[136] reported an intelligent O_2-evolving PDT nanoparticle (CM-MMNPs). The nanostructure consists of a MnO_2 nanosheet-coated metal–organic framework and a cancer cell membrane. In the preparation process, MnO_2 nanoflakes were firstly prepared by the reaction of sodium citrate (organic salt) and $KMnO_4$. In the organic reduction method, most of the micromolecular organics are bio-friendly reagents, and have applications such as physiological buffer, anticancer drugs, and food additives. Except for micromolecular organics, $KMnO_4$ also can be reduced by macromolecules, such as polymers and protein.[132,137,138] The selected polymers include poly (allylamine hydrochloride) (PAH), polyethylene glycol (PEG), hydroxylated polyethylene glycol, and polydiallydimethylammonium chloride (PDDA).[69,77,132,139] Currently, PAH is one of the most commonly used reduction agents.[140,141] Typically, Prasad *et al.*[37] designed and synthesized a MnO_2 nanoparticle–albumin conjugate (A-MnO_2). In the process, the MnO_2 nanoparticles were prepared by the redox reaction between $KMnO_4$ and cationic polyelectrolyte PAH. The size of MnO_2 nano-

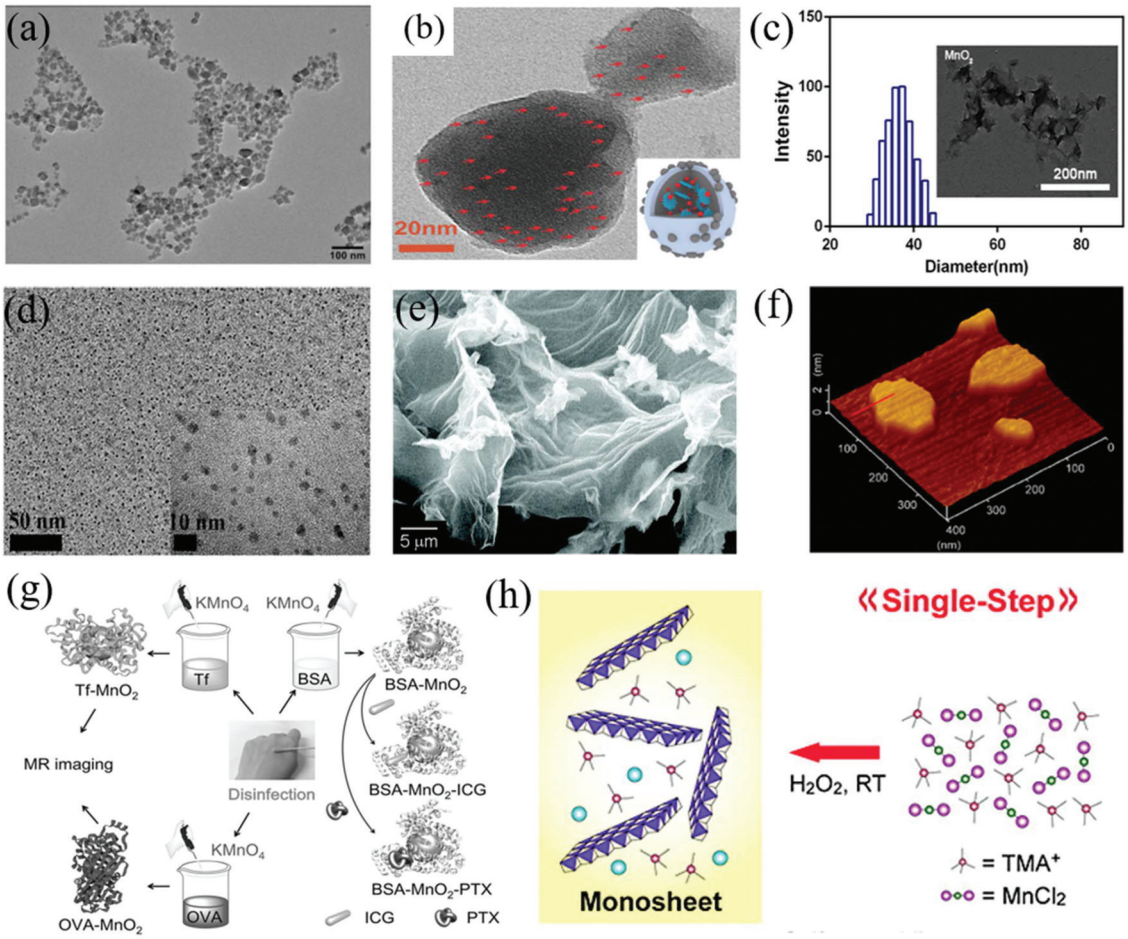

Fig. 4 (a) TEM image of $sMnO_2$. Reproduced with permission from ref. 128. Copyright 2019 WILEY-VCH Verlag GmbH & Co. KGaA, Weinheim. (b) The TEM image and schematic illustration of an individual FMZ/DC. Reproduced with permission from ref. 129. Copyright 2018 WILEY-VCH Verlag GmbH & Co. KGaA, Weinheim. (c) Size distribution and TEM image of MnO_2. Reproduced with permission from ref. 38. Copyright 2019 American Chemical Society. HRTEM image (d) of BM NPs and the synthetic procedure (g) of an MnO_2 NP-based theranostic platform. Reproduced with permission from ref. 138. Copyright 2016 WILEY-VCH Verlag GmbH & Co. KGaA, Weinheim. SEM image (e), AFM image (f), and synthetic procedure (h) of MnO_2 monosheets. Reproduced with permission from ref. 125. Copyright 2008 American Chemical Society.

particles was *ca.* 15 nm. This synthesis procedure has many advantages such as rapidity, satisfactory repeatability, and good stability. As a complement, Lu *et al.*[139] designed a nanosearchlight based on MnO_2 nanotubes for imaging multiple microRNAs. In the process, poly(diallydimethylammonium chloride) (PDDA) was used to reduce $KMnO_4$ as a reductant and stabilizer. Some proteins also can be selected to prepare nanostructured MnO_2 by reducing $KMnO_4$.[133,142] Recently, Pan *et al.*[138] proposed an ultra-simple method to prepare biomimetic nanoprobes by simulating the disinfection process of $KMnO_4$. As shown in Fig. 4g, the BSA was selected as a reductant under mild conditions. Briefly, $KMnO_4$ was mixed with BSA to generate MnO_2 nanoparticles in an aqueous solution. Finally, a multifunctional BSA-MnO_2 nanoparticle (BM NPs) was prepared. The prepared BM NPs had a sphere-like geometry with a uniform size of *ca.* 2.9 nm (Fig. 4d). The preparation strategy has many advantages, such as an ultra-facile procedure, low cost, mild synthesis conditions, and energy-saving nature.

2.3.2 Mn^{2+} ($MnCl_2$) oxidation method. Based on the redox principle, another representative preparation method is the Mn^{2+} ($MnCl_2$) oxidation method. At present, the Mn^{2+} ($MnCl_2$) oxidation method is being widely used to prepare nanostructured MnO_2 for anticancer applications.[143,144] The most representative method was first proposed by Kai *et al.*[125] in 2008. The method was widely used to prepare single-layer MnO_2 nanosheets for anticancer applications. In the preparation process, Mn^{2+} ($MnCl_2$) was oxidized with H_2O_2 (Fig. 4h) in the presence of TMA·OH. In the past, the preparation of single-layer MnO_2 nanosheets depended on multi-step treatment, including high-temperature solid-state synthesis of bulk templates, ion-exchange, and exfoliation reactions in solutions. Delightingly, the MnO_2 nanosheet can be directly obtained in a single step by chemical oxidation of Mn^{2+} ions. Moreover, the highly efficient reaction is easy to carry out within a day at room temperature. SEM (Fig. 4e) and atomic force microscopy (AFM) (Fig. 4f) images showed that MnO_2 was sheet-like. The lateral dimensions of the sample were in

the range of 50–500 nm. With extensive research on the anticancer application, the efficient method without high-temperature treatment has been used more and more. Except for the preparation method proposed by Kai, there are also some other similar methods by oxidizing $MnCl_2$. It is worth mentioning that, Gu *et al.*[145] prepared a multifunctional upconversion nanoparticle (UCNP) based nanoplatform by coating MnO_2 on CaF_2:Yb,Er@silica nanoparticles. In order to obtain MnO_2 shells, Mn^{2+} ions were absorbed into CaF_2:Yb,Er@silica pores (negative charge). Afterward, sodium hydroxide was added to adjust the pH value. In an additional 2 h, heterogeneous CaF_2:Yb,Er@silica@MnO_2 core–shell nanoparticles were obtained.

2.4 Others

Besides the above-mentioned bio-mineralization method, template method, and redox method, there are also some other methods. In the field of anticancer therapy, two-dimensional (2D) MnO_2 nanosheets have been widely studied due to their good biocompatibility, stability, and multifunctionality. Recently, Wang *et al.*[41] fabricated an ultrathin MnO_2 nanosheet *via* a hydrothermal process. Briefly, $KMnO_4$ was added to water under stirring. Subsequently, the solution was moved into a Teflon-lined autoclave. After that, the temperature was raised to 180 °C for 2 h. Then, the prepared MnO_2 nanosheets were washed with water and dried under vacuum at 60 °C. In order to prevent the degradation of SnTe in blood circulation, Zhang *et al.*[146] prepared a novel ultrathin SnTe@MnO_2-SP nanosheet for tumor diagnosis and therapy. In the preparation process, the prepared SnTe nanosheets were coated with a MnO_2 shell *via* surface mineralization and the liquid precipitation method. Afterward, the SnTe@MnO_2 nanosheets were modified with soybean phospholipid (SnTe@MnO_2-SP). The multifunctional diagnosis and treatment nanoplatform has opened up an exciting research direction in anticancer applications.

In this section, we have summarized the main preparation methods of nanostructured MnO_2 for anticancer applications including the bio-mineralization method, template method, redox method, and some other methods. Although the preparation of nanostructured MnO_2 has made significant progress, it is still essential to further explore novel preparation methods, and better regulate some influencing factors, such as the morphology, structure, and specific surface area.

3. Anticancer applications of nanostructured MnO_2

Both theoretical and experimental research studies proved that nanostructured MnO_2 has high hemo-/histo-compatibility. To date, nanostructured MnO_2 has been used in many fields of biomedical applications.[22,88] In particular, the nanostructured MnO_2 has shown great prospects in anticancer applications due to its unique nanostructure and physicochemical properties.[147,148] Notably, publishing of papers on cancer diagnosis and treatment has been on a continuously rising trend in the past few years. Therefore, it is necessary to present the recent achievements and progression of nanostructured MnO_2 for anticancer applications.[149–152] In this section, we mainly summarize and evaluate anticancer applications in diagnosis and therapy.

3.1 Photodynamic therapy (PDT)

As a new therapeutic modality, PDT has been playing an increasingly important role compared with conventional methods such as surgery, chemotherapy, and radiotherapy.[153,154] The so-called PDT refers to a treatment method with photosensitive drugs and laser activation.[155–159] Unfortunately, the uncontrolled proliferation of tumor cells and oxygen consumption during PDT always lead to insufficient oxygen levels, which attenuates PDT efficiency in turn.[32,160] Meanwhile, some harmful metabolites (such as H_2O_2) can be produced in the process of hypoxia.[65,161] Fortunately, nanostructured MnO_2 can be used effectively to enhance PDT by its reaction with some harmful substances (*e.g.*, H^+, H_2O_2, *etc.*). In recent years, nanostructured MnO_2 has been widely explored in PDT.[65,66] Therefore, several representative examples will be highlighted according to the enhanced principle.

3.1.1 Reduce GSH to enhance PDT. PDT is a promising and approved approach for tumor treatment.[162,163] However, current PDT still faces several obstacles.[52,163] As shown in Fig. 5a, GSH is at least four times higher in tumor cells than that in normal cells.[50] Notably, the concentration of GSH is also 100–1000-fold higher in the intracellular fluid than in the extracellular fluid.[51] As an enemy of PDT, the high reduced GSH concentration will hinder the clinical applications due to the occurrence of ROS consumption. Therefore, it is necessary to reduce the GSH level for improving the PDT efficiency.[164,165] In order to overcome the obstacle and enhance the therapeutic effect, researchers have proposed many strategies.[166–168] It is gratifying to note that the GSH can be reduced to improve the PDT efficiency by reaction with MnO_2. The mechanism is shown in eqn (1)

$$2GSH + MnO_2 + 2H^+ \rightarrow GSSG + Mn^{2+} + 2H_2O \quad (1)$$

Considering the additional GSH obstacle during the PDT, Min *et al.*[169] prepared a porphyrinic Zr-metal–organic framework nanoparticle (Fig. 5b), which was used as a photosensitizer and drug carrier. In order to consume GSH, the Zr-metal–organic framework nanoparticles were encapsulated with MnO_2 before decorating with the tumor cell membrane. The PDT and anti-angiogenesis drugs can significantly improve the tumor inhibition efficiency after intravenous administration. The GSH assay in 4T1 cells was performed before and after nanoparticle treatment for 5 h. The GSH level in 4T1 cells decreased more than 50% after being treated with aMM and aMMTm (Fig. 5c). The results showed that the MnO_2 shell of aMMTm can effectively consume GSH in tumor cells and enable GSH-triggered drug release. More interestingly, Fan *et al.*[170] prepared a photosensitizer-MnO_2 nanosystem (Fig. 5d)

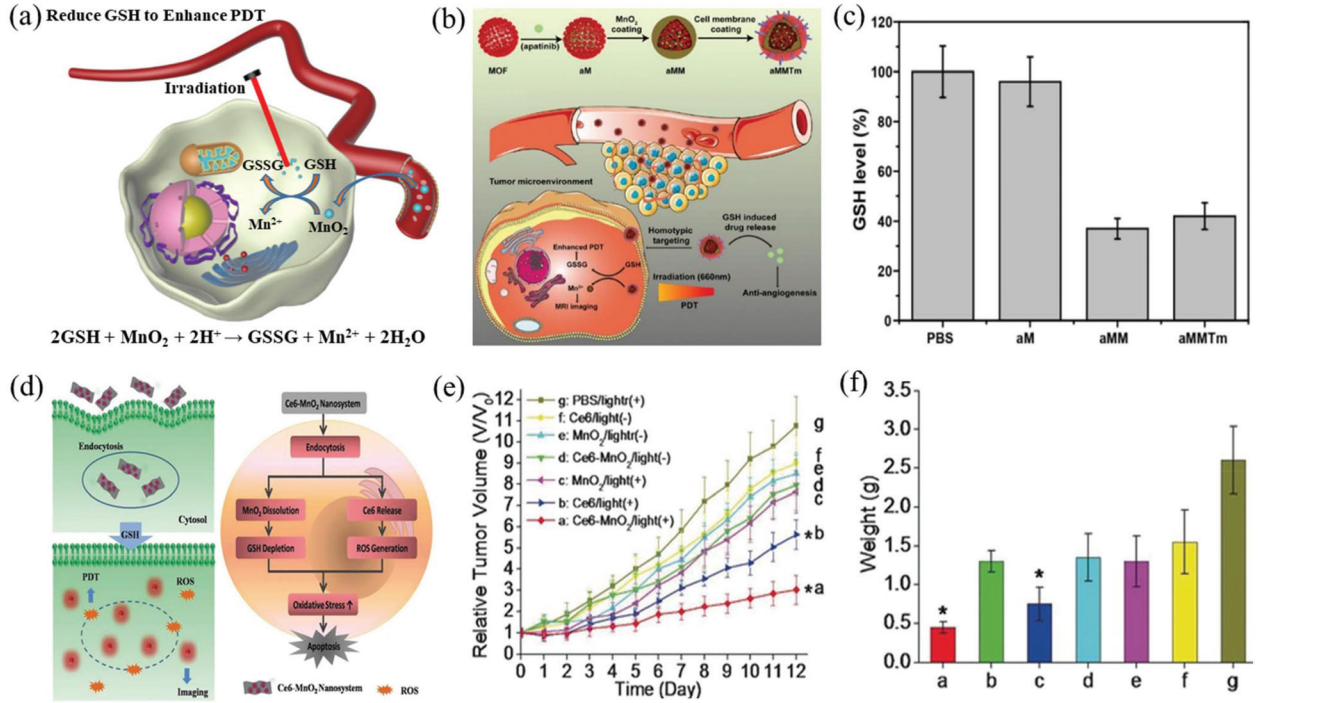

Fig. 5 (a) Schematic illustration of reducing the GSH level to improve the PDT effect in tumor cells. (b) Schematic illustration of aMMTm preparation and therapy. Reproduced with permission from ref. 169. Copyright 2019 WILEY-VCH Verlag GmbH & Co. KGaA, Weinheim. (c) The GSH level of 4T1 cells after treatment with PBS, aM, aMM and aMMTm for 5 h. Reproduced with permission from ref. 169. Copyright 2019 WILEY-VCH Verlag GmbH & Co. KGaA, Weinheim. (d) Schematic illustration of the Ce6–MnO_2 nanosystem for highly efficient PDT. Reproduced with permission from ref. 170. ©2016 WILEY-VCH. Tumor growth curves (e) and weights (f) of different tumor groups after treatment. Reproduced with permission from ref. 170. Copyright 2016 Wiley-VCH Verlag GmbH & Co. KGaA, Weinheim.

by adsorbing chlorin e6 (Ce6) onto MnO_2 nanosheets. Once ingested by tumor cells, MnO_2 nanosheets not only can protect photosensitizers from light self-destruction but also can be reduced by intracellular GSH. Therefore, the nanosystem was decomposed to release Ce6, reduce the GSH level, and achieve efficient PDT. They evaluated the therapeutic effect of Ce6, MnO_2, and Ce6-MnO_2 nanosheets by monitoring the growth rate of the tumor. The experimental results showed that the Ce6–MnO_2 nanosheet treatment group had higher efficacy compared with the free Ce6 or MnO_2 nanosheet treatment group (Fig. 5e). The weights of these mice in different groups are shown in Fig. 5f. These results clearly showed that the PDT of the Ce6-MnO_2 nanosystem is enhanced. The Ce6-MnO_2 nanosheet can not only enhance the absorption of Ce6, but also reduce the intracellular GSH level to enhance the PDT effect.

3.1.2 Generate O_2 to enhance PDT. It is well known that malignant tumor cells are mildly acidic due to severe glycolysis.[61,62] Besides, a large amount of H_2O_2 is generated and accumulated during cell carcinogenesis. Unfortunately, the H_2O_2 can cause persistent oxidative stress and DNA oxidative damage.[64] Therefore, the microenvironment of the solid tumor is acidic and H_2O_2-rich compared with the normal cells.[171–173] Delightingly, MnO_2 can be decomposed into water-soluble Mn^{2+} ions (Fig. 6a). Mn^{2+} can be used for tumor recognition and diagnosis.[91] Meanwhile, MnO_2 and H_2O_2 can generate O_2 during the reaction process as shown in eqn (2):

$$\begin{aligned} &MnO_2 + 2H^+ \rightarrow Mn^{2+} + H_2O + 1/2O_2, \\ &MnO_2 + H_2O_2 + 2H^+ \rightarrow Mn^{2+} + 2H_2O + O_2 \end{aligned} \quad (2)$$

The generated O_2 was used to provide the necessary conditions, which can help achieve a better PDT effect in the as-described tumor microenvironment.[67,77,174–176] In order to overbear the hypoxia-related resistance in PDT, Liu *et al.*[177] prepared a nanoplatform (R-MnO_2-FBP) to monitor oxygen self-supply, enhance PDT, and feed back the therapeutic result. As raw materials, Rhodamine B (RhB)-encapsulated MnO_2 (R-MnO_2) and functionalized black phosphorus (FBP) were assembled. The results showed that the released O_2 was proportional to the release of Mn^{2+} and RhB in the nanoplatform. After being transported to the tumor cells, R-MnO_2-FBP was decomposed in the acidic and H_2O_2-rich microenvironment. Meanwhile, the produced O_2 was used to overcome hypoxia-related PDT resistance. Considering the nanostructured MnO_2 and tumor microenvironment, Kapri *et al.*[178] successfully designed a unique two-dimensional hybrid nanoplatform (p-MoS_2/n-rGO-MnO_2-PEG). The hybrid nanoplatform showed excellent performance as an O_2 self-sufficient PDT agent. As shown in Fig. 6b, MnO_2 nanoparticles increased intracellular O_2 to overcome the hypoxic conditions *via* the reaction with

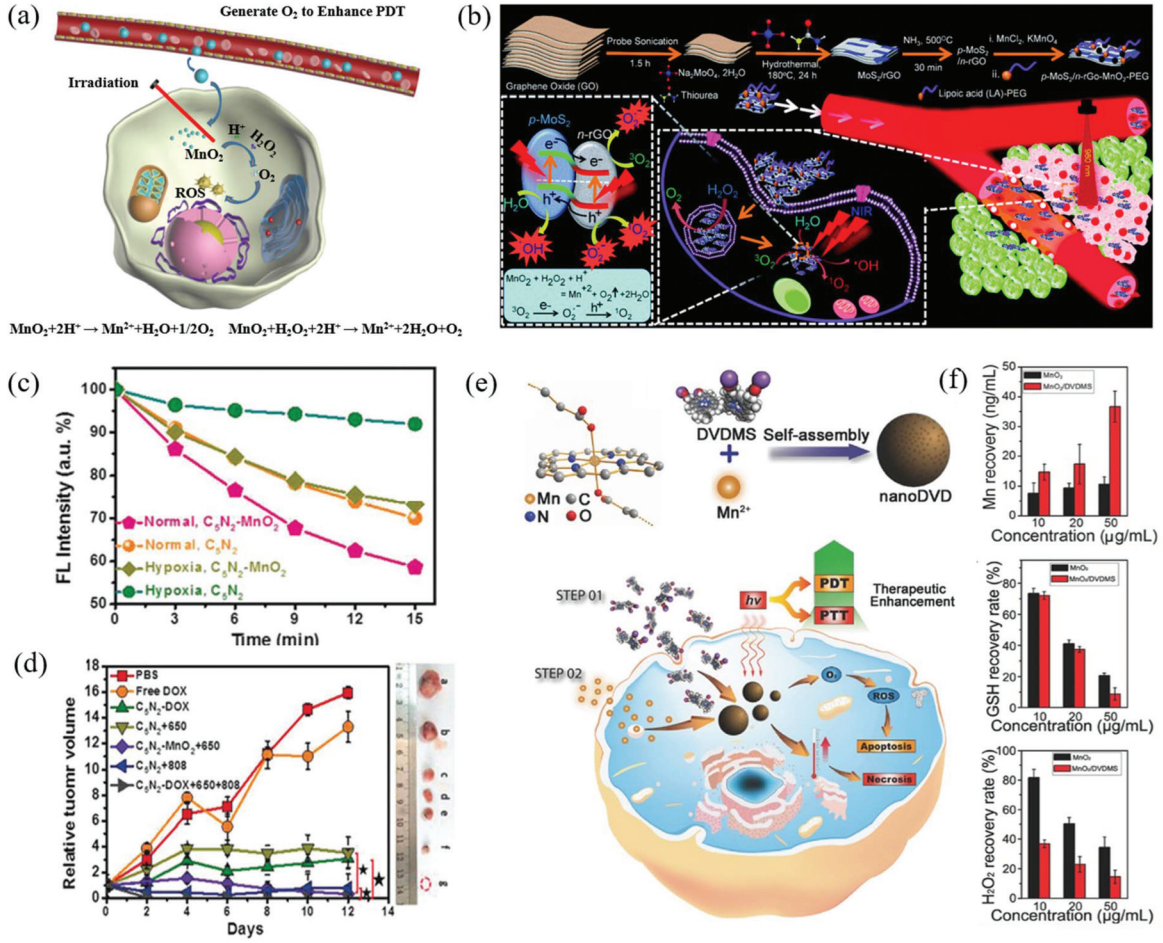

Fig. 6 (a) Schematic illustration of generating O_2 to improve the PDT effect in tumor cells. (b) Schematic illustration of the fabrication and application of p-MoS_2/n-rGO-MnO_2-PEG nanosheets. Image (b) from ref. 178. S. Kapri and S. Bhattacharyya, *Chem. Sci.*, 2018, **9**, 8982–8989. Reproduced with permission from the Royal Society of Chemistry, copyright 2018. Normalized fluorescence of C_5N_2 and C_5N_2–MnO_2 NPs under normal conditions or hypoxia (c), and relative tumor volumes and photographs with different treatments (d). Reproduced with permission from ref. 179. Copyright 2019 Wiley-VCH Verlag GmbH & Co. KGaA, Weinheim. (e) Schematic illustration of the PDT/PTT procedure of MnO_2/DVDMS. (f) The amount of Mn, GSH, and H_2O_2 recovery after the cells were cultured with MnO_2 and MnO_2/DVDMS. Images (e and f) from ref. 181. C. C. Chu, H. R. Lin, H. Liu, X. Y. Wang, J. Q. Wang, P. F. Zhang, H. Y. Gao, C. Huang, Y. Zeng, Y. Z. Tan, G. Liu and X. Y. Chen, *Adv. Mater.*, 2017, **29**, 1605928. Reproduced with permission from Wiley-VCH Verlag GmbH & Co. KGaA, Weinheim.

endogenous H_2O_2. The nanoplatform has been demonstrated to be a PDT photosensitizer *in vitro* for cancer therapy. Taking another recent design as an example, Chen *et al.*[179] accomplished a novel direct-nucleus-delivery nanoplatform based on C_5N_2 and MnO_2 nanoparticles. The PDT effect was restricted by hypoxia, because C_5N_2 nanoparticles inherently employ O_2 to generate singlet oxygen. MnO_2 nanoparticles were employed to produce O_2 by catalyzing the decomposition of overproduced H_2O_2 in the tumor microenvironment. As expected, the C_5N_2–MnO_2 nanoparticles produced more singlet oxygen (Fig. 6c) than C_5N_2 nanoparticles under hypoxia and effective therapeutic activity *in vivo* (Fig. 6d).

3.1.3 Synergistically enhance PDT. Some studies have combined GSH consumption with O_2 production to achieve a better PDT enhancement effect.[60,180] As a demonstration, Chu *et al.*[181] explored the conditions to form a therapeutic nanoagent based on clinical anti-tumor photosensitizer sinoporphyrin sodium (DVDMS) and Mn^{2+} (Fig. 6e). In such a novel design, MnO_2 nanosheets were not only used as delivery vectors for DVDMS but also employed as nanostructure generators for O_2 and DVDMS *in vivo*. The MnO_2/DVDMS was decomposed and assembled into DVDMS nanostructures by GSH and H_2O_2. According to the tests of an MCF-7 cell model and a tumor-bearing mouse model, GSH and H_2O_2 levels were reduced (Fig. 6f) with the effective internalization of MnO_2/DVDMS and MnO_2. The experiments revealed that the decrease of GSH, the generation of O_2, and the re-formation of DVDMS nanostructures were the main mechanisms significantly improving the optical therapy effect. Furthermore, Cheng *et al.*[180] introduced a preparation strategy to obtain a novel nanodevice and synergistically enhance PDT. First, they prepared some new composite photosensitizers by mixing DNA G-quadruplexes with hydrophilic porphyrin $(TMPipEOPP)^{4+}\cdot 4I^-$. Afterward, the prepared photosensitizers

were assembled with MnO_2 nanosheets. It not only showed high $^1O_2$ generation efficiency but also overcame the non-ideal consumption of GSH. The nanodevices have shown great potential in improving PDT efficiency both *in vitro* and *in vivo*. Similarly, Bi *et al.*[171] also developed a new biodegradable nanoplatform (MnO_2-Pt@Au_{25}) to improve the PDT effect by consuming GSH and generating O_2. In the nanoplatform, MnO_2 nanosheets anchored photodynamic agents (Au_{25} nanoclusters) and platinum(IV) precursors. Besides, MnO_2 nanosheets were endowed with the ability to consume GSH in tumor cells. As expected, the therapeutic effect was effectively improved along with the reduction of the GSH concentration.

In recent years, great progress has been made in basic research studies. As is known, nanostructured MnO_2 has broad prospects in the field of PDT due to its excellent properties. In our opinion, it will be conducive to optimize personalized schemes for different tumors and patients by revealing the structure–activity relationship of GSH consumption, $^1O_2$ production, and structure. Besides, it is important to further improve its selectivity and specificity in the future. Although it shows excellent performances in PDT, the potential risks, biological toxicity, and metabolic mechanisms are still necessary to be studied. Therefore, the toxicity should be reduced sufficiently on the premise of maintaining the therapeutic effect. Finally, researchers should establish a reliable standard for dose–response by carrying out long-term efficacy evaluation. As a new target treatment, PDT has been gradually recognized and promoted in clinical applications, and nanostructured MnO_2 is expected to play a more important role in PDT.

3.2 Bioimaging and cancer diagnosis (BCD)

Bioimaging technology is an important research method for tumor recognition and diagnosis.[182–184] People can observe the structure and distribution of tumor tissues *via* different imaging methods. The frequently used imaging modalities of tumors include MRI, computed tomography (CT), ultrasound scanning (US), fluorescence (FL), and photoacoustic (PA) imaging.[90,185] However, they often provide insufficient contrast and single imaging mode, although tumor imaging has a long history. At present, there is an urgent need to develop an ideal imaging material with multi-mode imaging function, high imaging contrast, and high chemical stability. In recent years, nanostructured MnO_2 has been creatively used in tumor imaging and diagnosis. Among them, excellent imaging performances have been verified in cells and animal models.

3.2.1 Magnetic resonance imaging (MRI). As we all know, MRI is one of the most attractive methods for tumor detection and diagnosis.[186–188] According to the published papers, the valence of Mn (MnO_2) is +4, and it does not show MRI performance. In contrast, Mn^{2+} has a strong ability of paramagnetic relaxation enhancement, which makes it play a role in the field of MRI contrast agents.[90,189] For the MRI application of Mn^{2+}, mangafodipir trisodium (Mn-DP-DP) is the first liver cell-specific MRI contrast agent in the world. Besides, it has obtained the Food and Drug Administration (FDA) certification. The Mn^{2+} contrast agent has obvious advantages: (1) there are various kinds of forms, such as chelates, oxides, and nanoparticles; (2) a small amount of Mn^{2+} can produce an obvious effect due to its strong paramagnetism; (3) the toxicity of the Mn^{2+} contrast agent is relatively low; and (4) the Mn^{2+} contrast agent can be used in neuroimaging. Fortunately, MnO_2 not only retains a stable state under neutral conditions but can also degrade under GSH/mildly acidic conditions.[190,191] It is even more meaningful to use the transformed Mn^{2+} for MRI in tumor sites.[192,193] Therefore, MnO_2 can be used as a contrast agent with excellent characteristics.[194–196] As a bioimaging nanoplatform, nanostructured MnO_2 has broad prospects.[197–200] Recently, some activated platforms based on nanostructured MnO_2 have been reported for bioimaging.[138,201–205] For instance, Meng *et al.*[206] described a ROS responsive nanoplatform (Fig. 7a) based on acriflavine and MnO_2 (ACF@MnO_2). From the dynamic MRI images in Fig. 7b, it can be seen that the signal intensity of the tumor area is 2.1-fold higher than that in the adjacent muscles at 4 h post-injection. The MR signal in the tumor area was weakened at 8 h post-injection. In contrast, the signal intensity of the kidney was enhanced between 8 and 36 h, indicating that Mn^{2+} was excreted through the kidney after being generated in tumor tissue. At the same time, the MR signal intensity of the liver hardly changed after injection. All these results indicate that ACF@MnO_2 can accumulate and enhance the T1-MR signal in the tumor site. In another work, Lin *et al.*[207] successfully prepared a novel nanoplatform (CuS_{NC}@DOX@$MnO_{2\text{-}NS}$), which was used for chemical and photothermal therapy under the guidance of multi-mode bioimaging. Among them, the MnO_2 nano-shell ($MnO_{2\text{-}NS}$) was decomposed into paramagnetic Mn^{2+} by GSH and H^+ in the tumor site. Then MRI and fluorescence imaging were triggered to locate the tumor. Under the guidance of multi-mode imaging, the combination of chemical therapy (DOX) and photothermal therapy (CuS_{NC}) have exhibited eminent efficiency in tumor ablation. Therefore, the nanoplatform can be precisely treated under the guidance of multi-mode imaging. In addition to these works, Revuri *et al.*[208] prepared oxygenic carbon nano-onion (CNO)/MnO_2 nanopods (iOCOMs). The Mn ions released from iOCOM during the catalysis of H_2O_2. The novel nanoparticles can reprogram the hypoxic tumor microenvironment and help achieve efficient hypoxia-triggered T1-MRI image-guided photothermal therapy.

3.2.2 Sensor for cancer diagnosis (SCD). Nanostructured MnO_2 has been widely used for the construction of biosensors based on its oxidizing ability and catalytic activity.[209,210] The biosensors can be classified into FL biosensors, electrochemical biosensors, and colorimetric biosensors.[23,90] In the tumor microenvironment, nanostructured MnO_2 can be decomposed into Mn^{2+} ions. Moreover, it has the properties of strong optical absorption and fast electron transfer. Therefore, it can be used as a fluorescence quenching agent in fluorescence analysis. Currently, it is being widely used to detect reduced substances in tumor sites.[211,212] First, the fluorescence was initially quenched by nanostructured MnO_2.

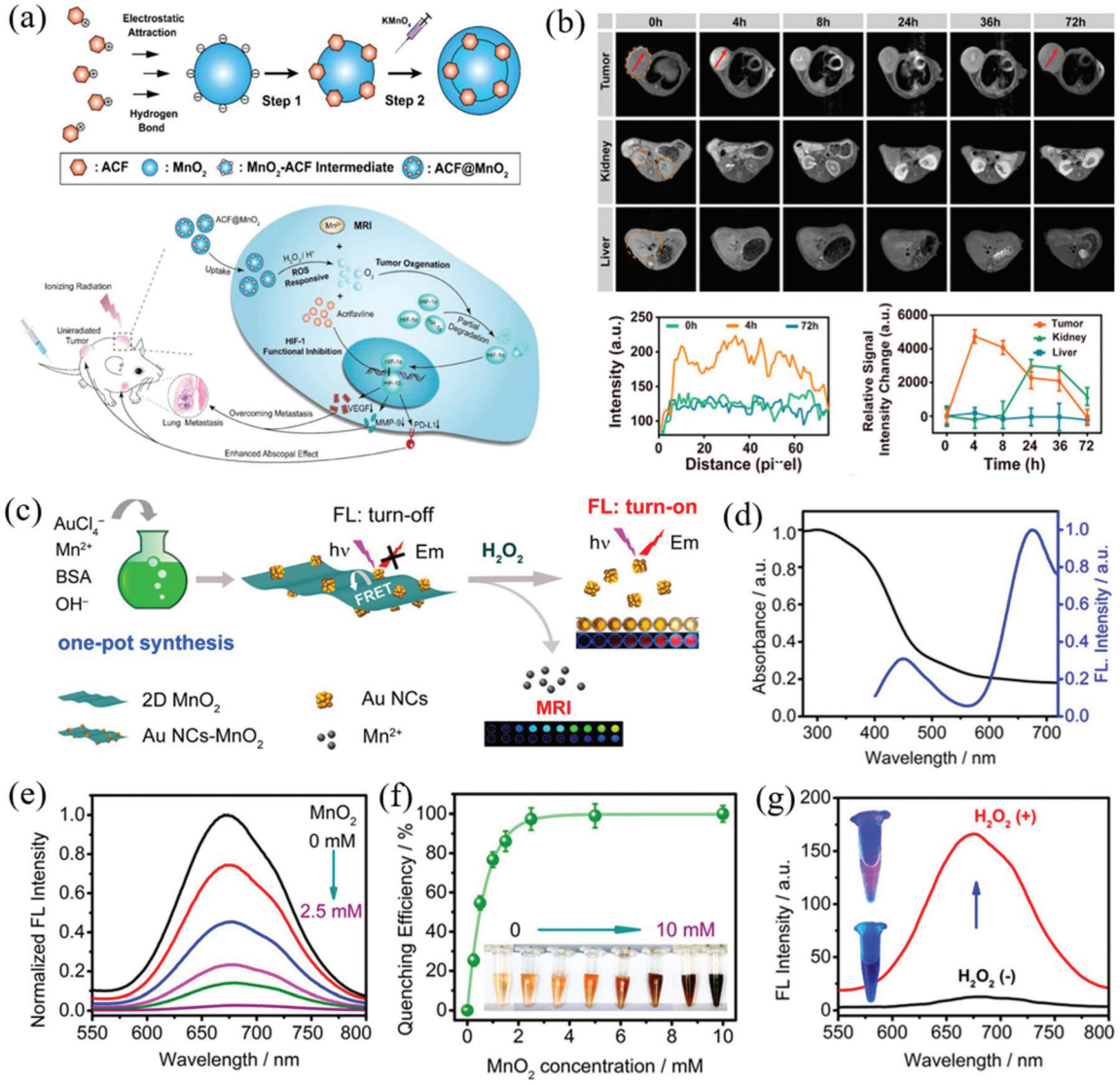

Fig. 7 (a) Schematic illustration of the fabrication and application of the ROS responsive nanoplatform. Reproduced with permission from ref. 206. Copyright 2018 American Chemical Society. (b) Dynamic MRI (top) after intravenous injection of ACF@MnO_2. Quantification (bottom-left) and relative signal change (bottom-right) of MR imaging intensity. Reproduced with permission from ref. 206. Copyright 2018 American Chemical Society. (c) Schematic representation for synthesis of Au NCs-MnO_2 nanosheets and H_2O_2 sensing. (d) UV-vis absorption spectrum of 2D MnO_2 (black line) and the fluorescence emission spectrum of Au NCs (blue line). (e) Normalized fluorescence emission spectra of Au NCs-MnO_2 at different MnO_2 concentrations. (f) Fluorescence quenching efficiency *vs.* concentrations of 2D MnO_2. (g) Fluorescence spectra of Au NCs-MnO_2 solution in the presence (red line) and absence (black line) of H_2O_2. Images in (c–g) were reproduced with permission from ref. 210. Copyright 2018 American Chemical Society.

Nanostructured MnO_2 would be further reduced to Mn^{2+} ions when it comes in contact with the reducing substance. Therefore, the fluorescent labels were released. Subsequently, the fluorescence was restored. By combining with different kinds of fluorescent nanomaterials, nanostructured MnO_2 can realize the recognition and diagnosis of the tumor by detecting the reducing substances (such as GSH).[213] Recently, Sheng *et al.*[210] reported a novel dual-mode fluorescent/magnetic sensor based on gold nanoclusters (Au NCs) and 2D MnO_2 nanosheets (Au NCs-MnO_2). In their design, a 2D MnO_2 nanosheet was selected as a quencher and recognizer in sensing platforms, respectively (Fig. 7c). Upon H_2O_2 introduction, the 2D MnO_2 nanosheet could be reduced to Mn^{2+} with rapid recovery of fluorescence. As shown in Fig. 7d, the UV-Vis absorption spectrum of the 2D MnO_2 nanosheet showed a strong wide absorption band (200–800 nm). The absorption/emission spectra of 2D MnO_2 and Au NCs were well matched, and therefore 2D MnO_2 can quench the fluorescence of Au NCs. As shown in Fig. 7e and f, the FL intensity of Au NCs was gradually quenched with the increase of 2D MnO_2. However, once hydrogen peroxide was added, the fluorescence intensity recovered rapidly due to the reduction of MnO_2 (Fig. 7g). The combination of Au NCs and MnO_2 provides a promising platform for the detection of H_2O_2 *in vivo*. Nanostructured MnO_2

has become a common sensor for cancer diagnosis due to its high catalytic activity, good biocompatibility, and high energy density. However, the conductivity of MnO_2 (10^{-6}–10^{-5} S cm^{-1}) is relatively low. Researchers usually produce sensors by combining MnO_2 with other superior conductivity materials. For instance, Wang *et al.*[214] reported a novel electrochemical immunosensor based on Co_3O_4@MnO_2-thionine (Co_3O_4@MnO_2-Th) for detecting alpha fetoprotein (AFP). The pseudo-enzyme-linked immunosorbent assay (pseudo-ELISA) method was used to prepare the immunosensor. A screen-printed carbon electrode (SPCE) was used to achieve detection. Meanwhile, amino functionalized Co_3O_4@MnO_2-Th was used as a secondary marker to improve the electrochemical response signal and detect AFP. The immunosensor has good selectivity, stability, and repeatability. Under the optimal conditions, the immunosensor has a linear response toward AFP in the range of 0.001–100 ng mL^{-1}, and the minimum detection limit is 0.33 pg mL^{-1}. The strategy opens a new way for the detection of tumor markers. In another work, Sun *et al.*[84] reported a sandwich-type electrochemical aptamer cytosensor (Fe_3O_4/MnO_2/Au@Pd) to detect human liver hepatocellular carcinoma cells (HepG2). After capturing the target cells, the aptamer cell composite nanoprobe was formed on the electrode surface. Then, the cytosensor not only efficiently catalyzed the oxidation of hydroquinone (HQ) with H_2O_2 (MnO_2) but also improved the sensitivity of detection by amplifying the electrochemical signal. The electrochemical sensor has many advantages, such as a wide detection range (1×10^2–1×10^7 cells per mL), high sensitivity, a low detection limit (15 cells per mL), good selectivity, and repeatability. Interestingly, the sensor can be regenerated by using the electrochemical reductive desorption method. These results indicated that the electrochemical cell sensor may be an effective tool for the early diagnosis of tumor cells.

In this section, we have introduced the research progress of nanostructured MnO_2 in tumor diagnosis. With its excellent physical and chemical properties, nanostructured MnO_2 has been widely used in MRI, SCD, and other diagnostic methods. However, it still faces many challenges: (1) Improvement of imaging sensitivity. The morphological structure is usually normal when the change of the lesion area is at the molecular level. Therefore, it is necessary to achieve an early diagnosis by improving imaging sensitivity. (2) Improvement of specificity. It is valuable to realize the rapid judgment of benign and malignant tumors by utilizing the characteristics of nanostructured MnO_2. (3) Improvement of safety. Biological metabolism and retention time should be reduced as much as possible.

3.3 Drug delivery system (DDS)

As to the application of the DDS, on the one hand, the nanostructured MnO_2 was used as a nanocarrier to load anticancer drugs.[120,215] On the other hand, it was selected as an intelligent "gatekeeper" to prevent early leakage of loaded drugs.[216,217] Interestingly, the protected drug only can be released with the degradation of MnO_2 in the tumor site. Compared with the traditional drug treatment pattern, the DDS has the following advantages: (1) it is easy to reduce the side effects of drugs; (2) it can change the half-life and extend the action time of drugs; (3) it can enhance the stability *in vivo* and *in vitro*; and (4) it can transport drugs to specific parts and reduce the damage to normal organs or tissues. In this section, we will mainly introduce the nanostructured MnO_2 in the DDS for anticancer applications.

3.3.1 Nanocarrier. With the increased concern on nanostructured MnO_2, it has been proved to be advantageous in the DDS for anticancer applications.[152,218,219] As shown in Fig. 8a, as a nanomaterial with large specific surface area, strong adsorption capacity, and good biocompatibility, various anticancer drugs can be loaded into the MnO_2 nanocarriers.[122,215,220] Besides, MnO_2 can be degraded in the tumor site with a mild acid and high GSH concentration.[221] Apparently, it is beneficial for drug release due to the degradability of MnO_2.[103,117,121,204] Lately, Tang *et al.*[222] designed a nanocarrier to enhance therapeutic efficacy (Fig. 8b). In their original work, an aza-BODIPY photosensitizer (SAB) was co-loaded with an anti-cancer drug (doxorubicin, DOX) onto MnO_2 nanoparticles, which have a large surface area and three-dimensional (3D) hydrangea-structure. Besides, the nanocarrier exhibited excellent tumor microenvironment responsiveness and degradability. In a mildly acidic microenvironment, the decomposition of MnO_2 was beneficial for the drug release.

3.3.2 Gatekeeper. As we all know, chemotherapy often causes systemic toxicity and side effects. To resolve this issue, it is particularly critical to avoid premature leakage of drugs in the DDS.[216,217] Therefore, MnO_2 was selected as a "gatekeeper" to prevent early leakage of the loaded drugs. For instance, Zhao and co-workers[108] prepared an intelligent nanocomposite ($PMAA_{BACy}$/DOX/MnO_2-2/PEG). Firstly, the poly(methacrylic acid-*co*-*N*,*N*-bis(acryloyl)-cystamine) ($PMAA_{BACy}$) nanohydrogels were cross-linked with disulfide to chelate the Mn^{2+} ions and load the chemotherapeutic drug (DOX). In this case, functional $PMAA_{BACy}$/DOX/MnO_2 was crafted *via* a biomineralization method, which induced the change of Mn^{2+} into amorphous MnO_2 at a mild temperature. MnO_2 served as a "gatekeeper" to prevent the premature leakage of DOX during blood circulation. Similarly, Feng *et al.*[204] prepared a magnetic iron carbide-glucose oxidase nanoparticle (Fe_5C_2-GOD@MnO_2) with high enzyme loading capacity (Fig. 8c). As an intelligent "gatekeeper", MnO_2 can prevent early leakage of glucose oxidase (GOD) before reaching the tumor tissue. After systemic administration, Fe_5C_2-GOD@MnO_2 nanocatalysts maintained inactivity in normal cells. In contrast, MnO_2 nanoshells decomposed into Mn^{2+} in the acidic microenvironment. Subsequently, O_2 and GOD were released. They studied the pharmacokinetics and biocompatibility, and the results are shown in Fig. 8d. The results showed that the nanocatalyst can effectively aggregate in the tumor site and exhibit a time-dependent clearance effect mainly by the liver and kidney.

In recent years, the excellent performances of MnO_2 provided an opportunity to improve the precise chemotherapy.

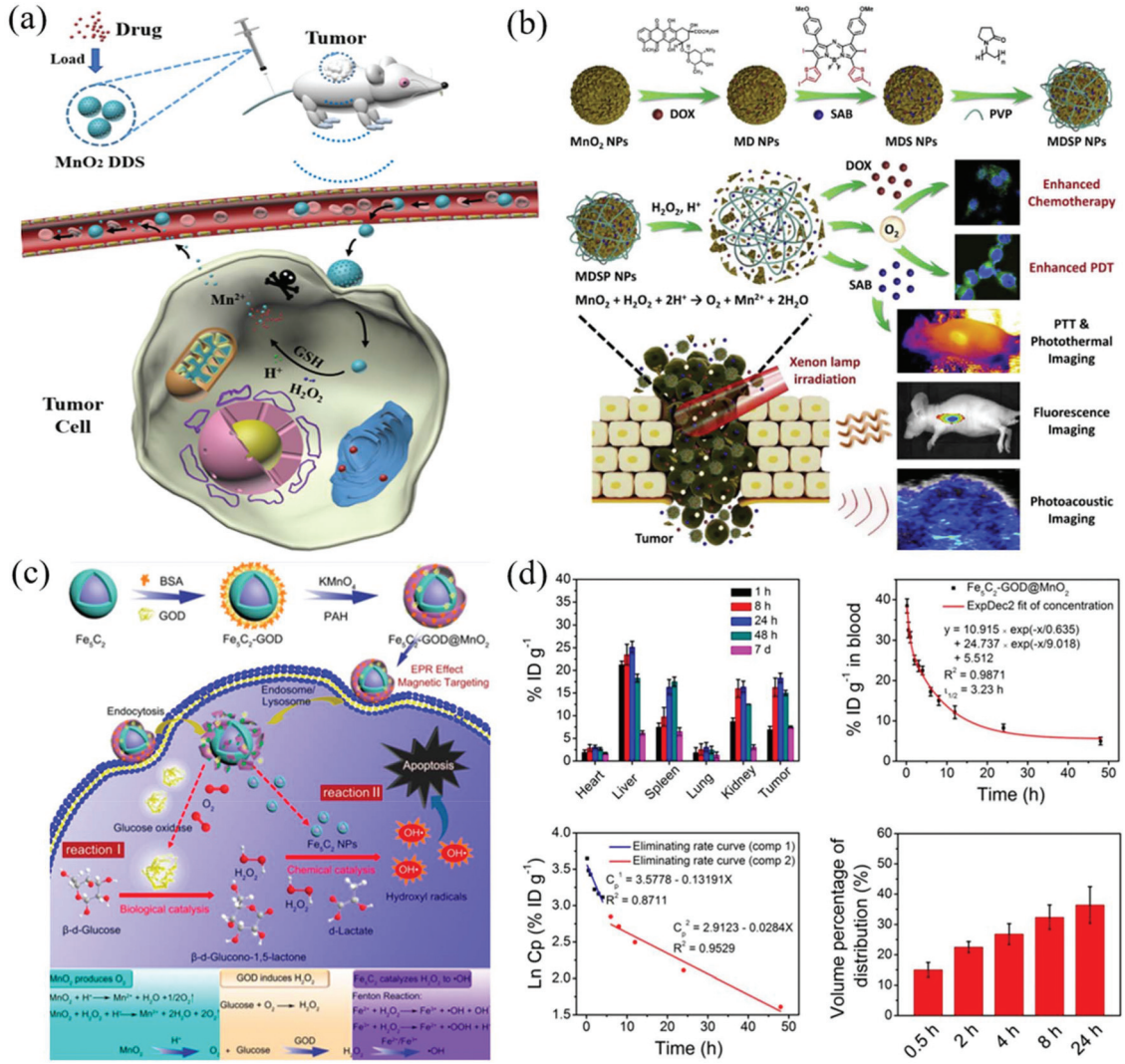

Fig. 8 (a) Schematic illustration of nanostructured MnO_2 for the drug delivery system. (b) Schematic illustration of the fabrication and applications of MDSP NPs. Reproduced with permission from ref. 222. Copyright 2019 Elsevier Ltd. (c) Synthetic process and therapeutic schematic of Fe_5C_2-GOD@MnO_2 nanocatalysts. (d) The biodistribution of Fe in main tissues and tumor, the blood circulation curve, the elimination rate curve, and the apparent volume percentage of distribution (V_d%) after intravenous administration of Fe_5C_2-GOD@MnO_2 nanocatalysts. Images in (c and d) were reproduced with permission from ref. 204. Copyright 2018 American Chemical Society.

Therefore, the MnO_2 based DDS has attracted extensive attention.[122,215,217,223] On the one hand, nanostructured MnO_2 was directly used to load drugs as a nanocarrier. On the other hand, it was selected as an intelligent "gatekeeper" to prevent early leakage of loaded drugs. However, there are still some challenges in the clinical applications: (1) controllable and advanced research on the commercial synthesis method is required; (2) it is essential to establish a complete real-time monitoring system; and (3) it is still necessary to study the potential risks, biological toxicity, and metabolic mechanism. In our opinion, there are some important factors to achieve the best treatment effect include accurate diagnosis, synchronous treatment, real-time monitoring, and adjustment of the drug given at any time. Therefore, the multifunctional DDS will develop towards the integration of diagnosis and treatment due to its excellent properties.

3.4 Other applications

There are also some other anticancer applications of nanostructured MnO_2 besides the three main therapies,[224] such as radiotherapy,[225] photothermal therapy (PTT), chemodynamic therapy (CDT), and improvement of the tumor microenvironment (Fig. 9a).[27,70,226–231]

3.4.1 Radiotherapy (RT). RT is one kind of mainstream method to kill tumor cells.[29] About half of the cancer patients have received radiotherapy at least once in the course of cancer treatment.[78,232] Radiotherapy can kill tumor cells *via* ionizing radiation. Ionizing radiation can directly destroy biological macromolecules, or convert intracellular oxygen (O_2) molecules into ROS.[233] However, the tumor tissue is usually characterized by hypoxia. Therefore, hypoxia is one of the main obstacles faced by radiotherapy. It is necessary to improve the local oxygen content of tumor tissue for enhancing radiotherapy.

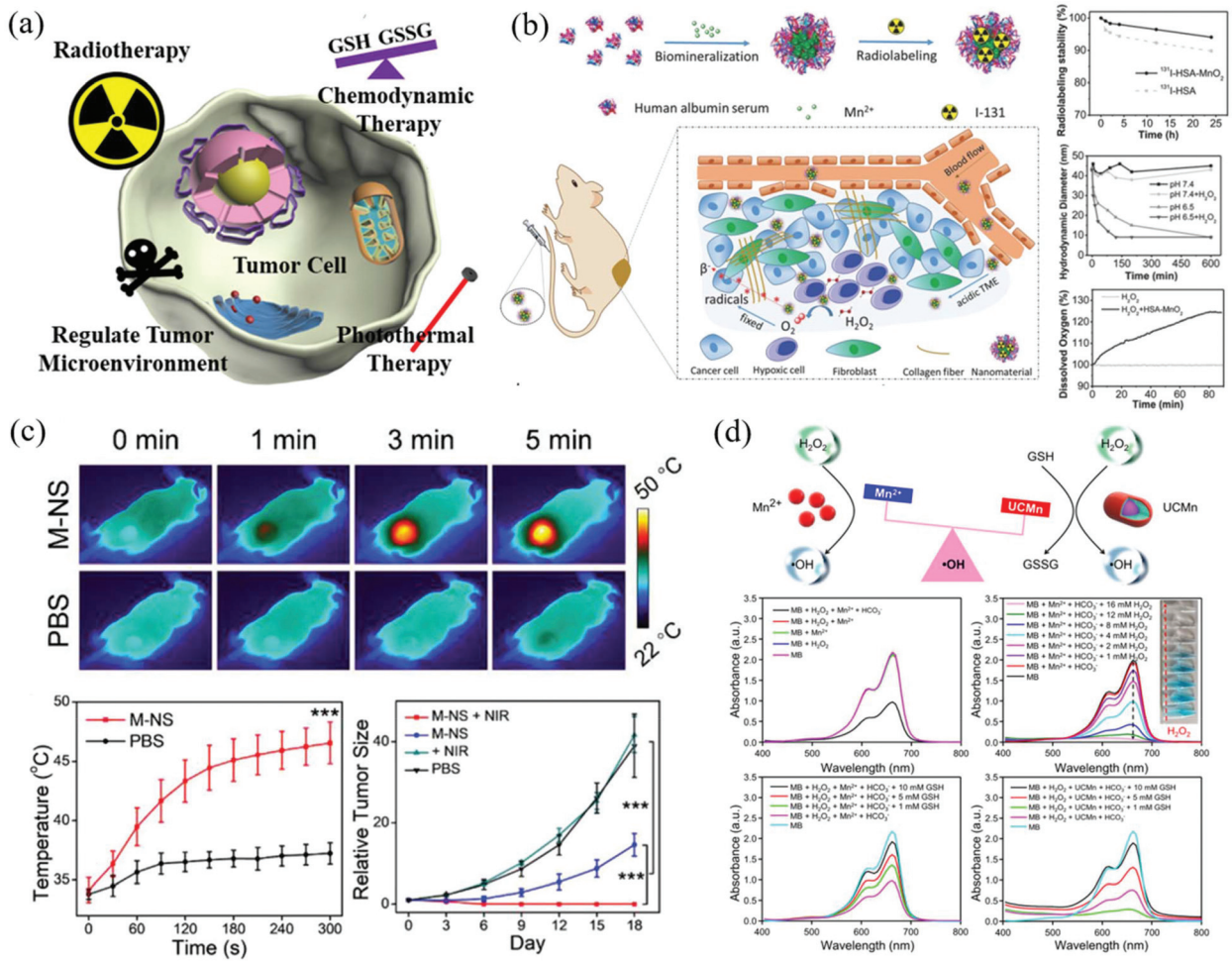

Fig. 9 (a) Schematic illustration of nanostructured MnO_2 for other various anticancer applications. (b) Preparation and characterization of ^{131}I-HSA-MnO_2 nanoparticles. Reproduced with permission from ref. 226. Copyright 2017 Wiley-VCH Verlag GmbH & Co. KGaA, Weinheim. (c) Thermographic images, temperature curves, and tumor growth curves of tumors. Reproduced with permission from ref. 236. Copyright 2019 WILEY-VCH Verlag GmbH & Co. KGaA, Weinheim. (d) MB degradation by Mn^{2+} or UCMn-mediated Fenton-like reaction. Reproduced with permission from ref. 238. Copyright 2019 American Chemical Society.

MnO_2 can rapidly improve the anoxia microenvironment by the decomposition of H_2O_2. Hence, it is a promising radiosensitizer, which will further improve the efficiency of radiotherapy.[78,233] Recently, a hybrid MnO_2 nanoparticle (MDNP) has been developed by Abbasi *et al.*[83] The nanoparticle can provide O_2 by reacting with endogenous H_2O_2. They found that the MDNP could not only regulate hypoxia and improve the radiotherapeutic effect but also reduce the expression of the vascular endothelial growth factor and vascular density. In the murine model, approximately 40% of tumor-bearing mice were tumor-free after a single treatment with MDNPs. Recently, Tian *et al.*[226] developed a new radioisotope therapy (RIT) nanoplatform (^{131}I-HSA-MnO_2) by combining radionuclide ^{131}I labeled HSA with MnO_2. The decomposition of endogenous H_2O_2 would be induced by MnO_2. The generated oxygen would be helpful in relieving hypoxia-associated RIT resistance of tumors. The radiolabeled stability of ^{131}I-HSA-MnO_2 was higher than that of ^{131}I-HSA, indicating that MnO_2 improved the radiolabeled stability (Fig. 9b). Moreover, the increase of oxygen after adding HSA-MnO_2 nanoparticles proved that these nanoparticles can effectively convert hydrogen peroxide into water and oxygen. Besides, the appropriate size of ^{131}I-HSA-MnO_2 nanoparticles enhanced the permeability and retention in blood circulation. In contrast, it showed little retention in other normal organs. Therefore, it showed fairly effective passive absorption to reduce radiotoxicity. They concluded that ^{131}I-HSA-MnO_2 nanoparticles could be used as an effective RIT agent in anticancer treatment.

3.4.2 Photothermal therapy (PTT). PTT is another promising approach to kill tumor cells.[79,132,137] Photothermal materials can convert light (especially NIR) into heat under irradiation.[75,234] With the rapid development of photothermal materials, some ultra-thin 2D nanosheets have shown unique physical, chemical, and biological effects.[23] Some recent studies have found that the ultra-thin 2D-MnO_2 nanosheets can be used as a new photothermal agent[235,236] due to their photothermal conversion ability. In order to improve the therapeutic effect of photothermal nanoagents, Liu *et al.*[235] devel-

oped a nanoparticle with tumor microenvironment hypersensitivity. They synthesized a supersensitive 2D-MnO_2 nanosheet for PTT. As expected, the MnO_2 nanosheets showed high photothermal conversion performance. The high PTT efficiency has been systematically demonstrated to inhibit the growth of tumors. Therefore, the photosensitizer has broadened the anticancer applications of functional biomaterials. Recently, Tang *et al.*[236] reported a novel method to synthesize 2-D MnO_2 nanosheets (M-NS_S). In their design, the size and thickness of M-NS_S can be easily adjusted *via* the dosage of protein. Afterwards, a unique sonochemical method was used to functionalize the surface of M-NS_S. Importantly, the well-designed M-NS_S also show excellent phototheranostic performance (Fig. 9c).

3.4.3 Chemodynamic therapy (CDT). CDT is a new therapeutic method, which can kill tumor cells by producing hydroxyl radicals ($^{\bullet}OH$) *in situ*.[26,237] The mitochondria, lipids, proteins, and DNA of tumor cells are irreversibly damaged. Importantly, it is not necessary to apply an external energy field. Therefore, CDT avoids the limitation of tissue penetration depth (such as laser) and side effects (various rays). Besides, MnO_2 can enhance the CDT effect by consuming GSH and producing more $^{\bullet}OH$. For instance, Ding *et al.*[238] developed a hybrid nanoplatform (UCMN) by coupling an upconversion nanoparticle (UCNP) and MnO_2. In their work, an ideal MnO_2 camouflage and tumor microenvironment triggering system was reported by growing MnO_2 on the surface of the UCNP. The complex structure significantly improved the efficiency of CDT through GSH consumption and cisplatin activation-enhanced $^{\bullet}OH$ generation. The –OH produced by MnO_2 mediated Fenton-like reaction depends on the concentration of H_2O_2 (Fig. 9d). MnO_2 can effectively alleviate the scavenging effect due to the consumption characteristics of GSH. Besides, the synergistic effect of CDT and chemotherapy was better than that of chemotherapy alone *in vivo*.

3.4.4 Regulation of the tumor microenvironment (RTM). RTM is a promising strategy to improve the effect of tumor therapy.[104] Some studies have shown that the deterioration and metastasis of tumors are related to the microenvironment.[239,240] Researchers have achieved better antitumor effects to resist tumor metastasis by regulating the tumor microenvironment such as O_2 production *in situ*.[113,241] In recent years, regulating the tumor microenvironment has been and is still one of the most promising measures for improving the therapeutic effect.[76,81] Some treatment measures have been significantly enhanced by improving the tumor microenvironment.[76,81,242] Recently, Gao *et al.*[231] constructed a modified hollow MnO_2 catalytic nanosystem for tumor immunotherapy. The produced O_2 has a sensitization effect on both extracellular and intracellular processes by the decomposition of endogenous H_2O_2. The results showed that the nanosystem could continuously remove lactic acid and produce a tumor microenvironment with immune activity. Besides, the regulation strategy can effectively improve the anti-cancer effect without using any immune agonists to avoid autoimmunity. Hypoxia relief of the tumor microenvironment can induce tumor cells to the S phase and enhance the sensitivity of chemotherapy. Guo *et al.*[241] developed a nanocarrier (CaM-PB), which can sequentially relieve hypoxia, change the physiological microenvironment, and control the drug release. MnO_2-loaded, bovine serum albumin (BSA) and PEG-comodified $CaSiO_3$ (CaM-PB) NPs were assembled for the engineering of the tumor microenvironment. 10-Hydroxycamptothecin (HCPT) was (S phase sensitive drug) loaded into nanocarriers. The results showed that MnO_2 could generate O_2 (react with H_2O_2), relieve hypoxia, change glycolysis mode, and increase the number of S phase cells in 8 h. Besides, HCPT continuously released for more than 60 h. Therefore, it not only effectively attacked the tumor cells in the S-phase but also enhanced the chemotherapy effect of the S phase sensitive drug (HCPT).

4. Summary and outlook

Nanostructured MnO_2 has attracted extensive attention in the field of anticancer therapy due to its many excellent properties. In this review, we have presented the recent achievements and progress of nanostructured MnO_2 for anticancer applications, including preparation methods, diagnosis, and treatments. Although many outstanding results have been achieved, most research studies of nanostructured MnO_2 are still at the primary stage. In our opinion, the anticancer applications of nanostructured MnO_2 still face many challenges. As shown in Fig. 10, the future trends and challenges may include the following aspects:

(I) *Clinical transformation*. Nanostructured MnO_2 has many potential anticancer applications due to its excellent properties. However, the main issues lie in their clinical transformation. Following basic research, MnO_2-based multi-functional nanomaterials are expected to have further clinical applications. Therefore, it is increasingly crucial to provide a practical and effective method to make the clinical transformation and application come true.

(II) *Enhance diagnostic accuracy*. Nanostructured MnO_2 has application prospects in tumor diagnosis, but finding ways to further improve the imaging sensitivity and specificity for anti-

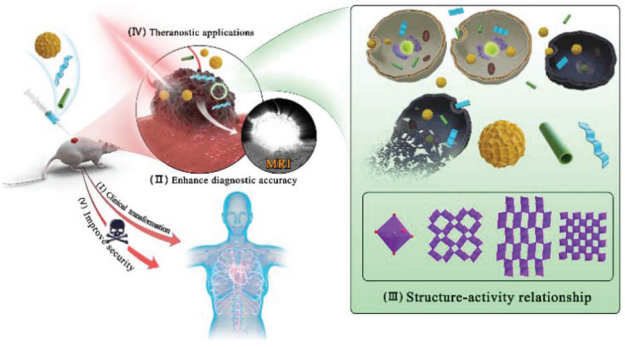

Fig. 10 Schematic illustration of nanostructured MnO_2 for future trends and challenges.

cancer diagnosis will be a challenge in the future. Based on the characteristics of nanostructured MnO_2, it is necessary to achieve early diagnosis by quantitative analysis. Besides, the specificity of the diagnosis is also of great significance for the rapid judgment of benign and malignant tumors.

(III) *Structure–activity relationship*. We think that revealing the detailed anticancer mechanism and structure–activity relationship of nanostructured MnO_2 will be conducive to optimization of personalized treatment schemes for different tumors. Besides, the improvement of selectivity and specificity in tumor treatment will also be a challenge in the future.

(IV) *Theranostic applications*. The excellent performances of nanostructured MnO_2 provide an opportunity to achieve a variety of diagnosis and treatment. Hence, some novel, controllable, and commercial preparation methods should be designed to obtain the functional MnO_2 nanostructure. It is conducive to achieve the best therapeutic effect by monitoring the therapeutic effect and adjusting the drug administration at any time. Therefore, the multi-functional nanoplatform will develop towards the direction of tumor diagnosis and treatment integration due to its excellent properties.

(V) *Improve security*. Although nanostructured MnO_2 shows excellent performance, the potential risks, biological toxicity, and metabolic mechanism are still unclear due to the short research time. It is necessary to understand the biosafety in detail. Therefore, the toxicity should be fully reduced on the premise of maintaining the therapeutic effect. Besides, researchers should make a long-term evaluation of the efficacy, and establish a more reliable dose–response reference standard.

Currently, nanostructured MnO_2 has great potential for anticancer applications, and there are infinite research opportunities to explore for researchers.

Abbreviations

2D	Two-dimensional
3D	Three-dimensional
AFM	Atomic force microscopy
AFP	Alpha fetoprotein
Au NCs	Gold nanoclusters
BCD	Bioimaging and cancer diagnosis
BSA	Bovine serum albumin
CDT	Chemodynamic therapy
Ce6	Chlorin e6
CT	Computed tomography
DA	Dopamine
DDS	Drug delivery system
DVDMS	Sinoporphyrin sodium
FDA	Food and drug administration
FL	Fluorescence
FTn	Ferritin nanocages
OA	Oleic acid
GOD	Glucose oxidase
GSH	Glutathione
HCPT	10-Hydroxycamptothecin
HepG2	Human liver hepatocellular carcinoma cells
H-MnO_2	Hollow manganese dioxide
hMnO_2	Honeycomb MnO_2
HRTEM	High resolution transmission electron microscopy
HSA	Human serum albumin
MES	2-(*N*-morpholino)ethanesulfonic acid
Mn-DP-DP	Mangafodipir trisodium
MnO_2	Manganese dioxide
$MnO_{2\text{-NS}}$	MnO_2 nano-shell
M-NS_S	MnO_2 nanosheets
MRI	Magnetic resonance imaging
PA	Photoacoustic
PAH	Poly(allylamine hydrochloride)
PDDA	Polydiallydimethylammonium chloride
PDT	Photodynamic therapy
PEG	Polyethylene glycol
PLGA	Poly(lactic-*co*-glycolic acid)
PTT	Photothermal therapy
PVP	Poly(vinylpyrrolidone)
RhB	Rhodamine B
RT	Radiotherapy
RIT	Radioisotope therapy
ROS	Reactive oxygen species
sMnO_2	Ultra-small MnO_2
SPCE	Screen-printed carbon electrode
TMA·OH	Tetramethylammonium hydroxide
UCNP	Upconversion nanoparticle
US	Ultrasound scanning

Conflicts of interest

The authors declare no conflict of interest.

Acknowledgements

This study was supported by the National Natural Science Foundation of China (Grant No.: 21978047 and 21776046), the Fundamental Research Funds for the Central Universities (Grant No.: 2242020K40033), and the Six Talent Peaks Project in Jiangsu Province (Grant No.: XCL-079).

Notes and references

1 F. Liu, L. Lin, Y. Zhang, S. Sheng, Y. B. Wang, C. N. Xu, H. Y. Tian and X. S. Chen, *Biomaterials*, 2019, **223**, 119470.
2 B. L. Li, M. I. Setyawati, L. Y. Chen, J. P. Xie, K. Ariga, C. T. Lim, S. G. Araj and D. T. Leong, *ACS Appl. Mater. Interfaces*, 2017, **9**, 15286–15296.
3 A. Bijelic, M. Aureliano and A. Rompel, *Angew. Chem., Int. Ed.*, 2019, **58**, 2980–2999.
4 D. L. Ni, D. W. Jiang, H. F. Valdovinos, E. B. Ehlerding, B. Yu, T. E. Barnhart, P. Huang and W. B. Cai, *Nano Lett.*, 2017, **17**, 3282–3289.

5 A. Naik, R. Rubbiani, G. Gasser and B. Spingler, *Angew. Chem., Int. Ed.*, 2014, **53**, 6938–6941.
6 X. J. Hu, K. Ogawa, S. Q. Z. Li, T. Kiwada and A. Odani, *Bull. Chem. Soc. Jpn.*, 2019, **92**, 790–796.
7 W. Guo, C. Yu, S. F. Li, Z. Wang, J. H. Yu, H. W. Huang and J. S. Qiu, *Nano Energy*, 2019, **57**, 459–472.
8 Q. Z. Zhang, D. Zhang, Z. C. Miao, X. L. Zhang and S. L. Chou, *Small*, 2018, **14**, 1702883.
9 Y. F. Xu, J. G. Liu, J. Wang, G. Y. Ma, J. H. Lin, Y. Yang, Y. W. Li, C. H. Zhang and M. Y. Ding, *ACS Catal.*, 2019, **9**, 5147–5156.
10 H. Q. Wang, S. Chen, Z. Wang, Y. Zhou and Z. B. Wu, *Appl. Catal., B*, 2019, **254**, 339–350.
11 M. A. Dallaston, C. J. Bettencourt, S. Chow, J. Gebhardt, J. Spangler, M. R. Johnston, C. Wall, J. S. Brusnahan and C. M. Williams, *Chem. – Eur. J.*, 2019, **25**, 9614–9618.
12 S. Biswas, I. Arief, S. S. Panja and S. Bose, *ACS Appl. Mater. Interfaces*, 2017, **9**, 3030–3039.
13 B. B. Liu, Y. B. Zhang, J. Wang, J. Wang, Z. J. Su, G. H. Li and T. Jiang, *Adv. Powder Technol.*, 2019, **30**, 302–310.
14 Y. Yang, J. Li, H. W. Zhang, L. C. Jin, F. Xu, G. W. Gan, G. Wang and D. D. Wen, *Ceram. Int.*, 2018, **44**, 19370–19376.
15 S. S. Danewalia, S. Kaur, N. Bansal, S. Khan and K. Singh, *J. Non-Cryst. Solids*, 2019, **513**, 64–69.
16 S. Y. Su, Y. Xu, Y. Wang, X. Y. Wang, L. Shi, D. Wu, P. C. Zou, A. Nairan, Z. Y. Lin, F. Y. Kang and C. Yang, *Chem. Eng. J.*, 2019, **370**, 330–336.
17 Y. H. Liu, Z. Y. Jiang and J. L. Xu, *ACS Appl. Mater. Interfaces*, 2019, **11**, 24047–24056.
18 T. Zhai, X. H. Lu, F. X. Wang, H. Xia and Y. X. Tong, *Nanoscale Horiz.*, 2016, **1**, 109–124.
19 L. Miao, J. L. Wang and P. Y. Zhang, *Appl. Surf. Sci.*, 2019, **466**, 441–453.
20 M. Y. Wu, P. F. Hou, L. N. Dong, L. L. Cai, Z. D. Chen, M. M. Zhao and J. J. Li, *Int. J. Nanomed.*, 2019, **14**, 4781–4800.
21 Y. T. Hu, Y. Wu and J. H. Wang, *Adv. Mater.*, 2018, **30**, 1802569.
22 S. Kumar, I. M. Adjei, S. B. Brown, O. Liseth and B. Sharma, *Biomaterials*, 2019, **224**, 119467.
23 J. Chen, H. M. Meng, Y. Tian, R. Yang, D. Du, Z. H. Li, L. B. Qu and Y. H. Lin, *Nanoscale Horiz.*, 2019, **4**, 321–338.
24 H. Lin, Y. Chen and J. L. Shi, *Chem. Soc. Rev.*, 2018, **47**, 1938–1958.
25 Y. L. Du, H. Liu, J. M. Liang, D. Y. Zheng, J. Li, S. B. Lan, M. Wu, A. X. Zheng and X. L. Liu, *Talanta*, 2020, **209**, 120524.
26 H. M. Wang, L. An, C. Tao, Z. Y. Ling, J. M. Lin, Q. W. Tian and S. P. Yang, *Nanoscale*, 2020, **12**, 5139–5150.
27 M. L. Song, T. Liu, C. R. Shi, X. Z. Zhang and X. Y. Chen, *ACS Nano*, 2016, **10**, 633–647.
28 F. Zhou, T. T. Zheng, E. S. Abdel-Halim, L. P. Jiang and J. J. Zhu, *J. Mater. Chem. B*, 2016, **4**, 2887–2894.
29 S. Y. Wang, Q. You, J. P. Wang, Y. L. Song, Y. Cheng, Y. D. Wang, S. Yang, L. F. Yang, P. S. Li, Q. L. Lu, M. Yu and N. Li, *Nanoscale*, 2019, **11**, 6270–6284.
30 K. Xu, Z. H. Zhao, J. F. Zhang, W. Xue, H. P. Tong, H. Liu and W. G. Zhang, *J. Mater. Chem. B*, 2020, **8**, 1507–1515.
31 Y. Zhang, O. Eltayeb, Y. T. Meng, G. M. Zhang, Y. Zhang, S. M. Shuang and C. Dong, *New J. Chem.*, 2020, **44**, 2578–2586.
32 N. Yang, W. Y. Xiao, X. J. Song, W. J. Wang and X. C. Dong, *Nano-Micro Lett.*, 2020, **12**, 15.
33 T. Yumak, D. Bragg and E. M. Sabolsky, *Appl. Surf. Sci.*, 2019, **469**, 983–993.
34 S. Gao, G. H. Wang, Z. N. Qin, X. Y. Wang, G. Q. Zhao, Q. J. Ma and L. Zhu, *Biomaterials*, 2017, **112**, 324–335.
35 Y. Seo, J. Leong, J. Y. Teo, J. W. Mitchell, M. U. Gillette, B. Han, J. Lee and H. Kong, *ACS Appl. Mater. Interfaces*, 2017, **9**, 35642–35650.
36 W. P. Fan, W. B. Bu, B. Shen, Q. J. He, Z. W. Cui, Y. Y. Liu, X. P. Zheng, K. Zhao and J. L. Shi, *Adv. Mater.*, 2015, **27**, 4155–4161.
37 P. Prasad, C. R. Gordijo, A. Z. Abbasi, A. Maeda, A. Ip, A. M. Rauth, R. S. DaCosta and X. Y. Wu, *ACS Nano*, 2014, **8**, 3202–3212.
38 X. Yang, Y. Yang, F. Gao, J. J. Wei, C. G. Qian and M. J. Sun, *Nano Lett.*, 2019, **19**, 4334–4342.
39 S. Kim, S. M. Ahn, J. S. Lee, T. S. Kim and D. H. Min, *2D Mater.*, 2017, **4**, 025069.
40 P. Liu, J. H. Ren, Y. X. Xiong, Z. Yang, W. Zhu, Q. Y. He, Z. S. Xu, W. S. He and J. Wang, *Biomaterials*, 2019, **199**, 52–62.
41 L. Wang, S. Y. Guan, Y. Z. W. Weng, S. M. Xu, H. Lu, X. M. Meng and S. Y. Zhou, *ACS Appl. Mater. Interfaces*, 2019, **11**, 6267–6275.
42 C. A. Choi, J. E. Lee, Z. A. I. Mazrad, I. In, J. H. Jeong and S. Y. Park, *J. Ind. Eng. Chem.*, 2018, **63**, 208–219.
43 Q. Zhou, S. Q. Shao, J. Q. Wang, C. H. Xu, J. J. Xiang, Y. Piao, Z. X. Zhou, Q. S. Yu, J. B. Tang, X. R. Liu, Z. H. Gan, R. Mo, Z. Gu and Y. Q. Shen, *Nat. Nanotechnol.*, 2019, **14**, 799–809.
44 W. H. Chen, R. L. G. Lecaros, Y. C. Tseng, L. Huang and Y. C. Hsu, *Cancer Lett.*, 2015, **359**, 65–74.
45 D. F. Quail and J. A. Joyce, *Nat. Med.*, 2013, **19**, 1423–1437.
46 C. H. Chang, J. Qiu, D. O'Sullivan, M. D. Buck, T. Noguchi, J. D. Curtis, Q. Y. Chen, M. Gindin, M. M. Gubin, W. van der, J. W. Gerritje, E. Tonc, R. D. Schreiber, E. J. Pearce and E. L. Pearce, *Cell*, 2015, **162**, 1229–1241.
47 M. A. Swartz, N. Iida, E. W. Roberts, S. Sangaletti, M. H. Wong, F. E. Yull, L. M. Coussens and Y. A. DeClerck, *Cancer Res.*, 2012, **72**, 2473–2480.
48 M. F. Chung, H. Y. Liu, K. J. Lin, W. T. Chia and H. W. Sung, *Angew. Chem., Int. Ed.*, 2015, **54**, 9890–9893.
49 R. Y. Zhou, H. M. Wang, Y. F. Yang, C. Y. Zhang, X. H. Dong, J. F. Du, L. Yan, G. J. Zhang, Z. J. Gu and Y. L. Zhao, *Biomaterials*, 2019, **189**, 11–22.

50 J. Q. Wang, X. R. Sun, W. W. Mao, W. L. Sun, J. B. Tang, M. H. Sui, Y. Q. Shen and Z. W. Gu, *Adv. Mater.*, 2013, **25**, 3670–3676.
51 R. Cheng, F. Feng, F. H. Meng, C. Deng, J. Feijen and Z. Y. Zhong, *J. Controlled Release*, 2011, **152**, 2–12.
52 S. Monro, K. L. Colon, H. M. Yin, J. Roque, P. Konda, S. Gujar, R. P. Thummel, L. Lilge, C. G. Cameron and S. A. McFarland, *Chem. Rev.*, 2019, **119**, 797–828.
53 M. H. Lan, S. J. Zhao, W. M. Liu, C.-S. Lee, W. J. Zhang and P. F. Wang, *Adv. Healthcare Mater.*, 2019, **8**, 1900132.
54 C. H. Liu, D. D. Wang, S. Y. Zhang, Y. R. Cheng, F. Yang, Y. Xing, T. L. Xu, H. F. Dong and X. J. Zhang, *ACS Nano*, 2019, **13**, 4267–4277.
55 J. Deng, F. Liu, L. N. Wang, Y. An, M. Gao, Z. Wang and Y. J. Zhao, *Biomater. Sci.*, 2019, **7**, 429–441.
56 H. M. Meng, D. Zhao, N. Li and J. B. Chang, *Analyst*, 2018, **143**, 4967–4973.
57 H. Zhang, K. Liu, S. K. Li, X. Xin, S. L. Yuan, G. H. Ma and X. H. Yan, *ACS Nano*, 2018, **12**, 8266–8276.
58 Y. D. Ruan, X. D. Jia, C. Wang, W. Y. Zhen and X. Jiang, *ACS Biomater. Sci. Eng.*, 2019, **5**, 1016–1022.
59 Y. Y. Deng, F. Jia, S. Y. Chen, Z. D. Shen, Q. Jin, G. S. Fu and J. Ji, *Biomaterials*, 2018, **187**, 55–65.
60 Y. W. Hao, B. X. Zhang, C. X. Zheng, M. Y. Niu, H. C. Guo, H. L. Zhang, J. B. Chang, Z. Z. Zhang, L. Wang and Y. Zhang, *Colloids Surf., B*, 2017, **151**, 384–393.
61 Y. L. Feng, Y. Cheng, Y. Chang, H. Jian, R. X. Zheng, X. Q. Wu, K. Q. Xu, L. Wang, X. M. Ma, X. Li and H. Y. Zhang, *Biomaterials*, 2019, **217**, 119327.
62 P. P. Liang, H. Tang, R. Gu, L. Xue, D. P. Chen, W. J. Wang, Z. Yang, W. L. Si and X. C. Dong, *Sci. China Mater.*, 2019, **62**, 1199–1209.
63 Z. Li, *Talanta*, 2020, **212**, 120804.
64 B. P. Ling, H. T. Chen, D. Y. Liang, W. Lin, X. Y. Qi, H. P. Liu and X. Y. Deng, *ACS Appl. Mater. Interfaces*, 2019, **11**, 11157–11166.
65 J. Zhang, M. Q. Xu, Y. L. Mu, J. J. Li, M. F. Foda, W. Y. Zhang, K. Han and H. Y. Han, *Biomaterials*, 2019, **218**, 119312.
66 D. D. Wang, H. H. Wu, W. Q. Lim, S. Z. F. Phua, P. P. Xu, Q. W. Chen, Z. Guo and Y. L. Zhao, *Adv. Mater.*, 2019, **31**, 1901893.
67 W. Pan, Y. G. Ge, Z. Z. Yu, P. Zhou, B. J. Cui, N. Li and B. Tang, *Chem. Commun.*, 2019, **55**, 5115–5118.
68 L. T. Meng, S. J. Gan, Y. Zhou, Y. L. Cheng, Y. W. Ding, X. N. Tong, J. H. Wu, Y. Q. Hu and A. Yuan, *Biomater. Sci.*, 2019, **7**, 168–177.
69 X. Li, X. Q. Feng, C. S. Sun, Y. X. Liu, Q. F. Zhao and S. L. Wang, *J. Controlled Release*, 2020, **319**, 104–118.
70 L. R. Zhao, C. H. Fu, L. F. Tan, T. Li, H. S. Zhong and X. W. Meng, *Nanoscale*, 2020, **12**, 2855–2874.
71 Y. G. Tao, L. L. Zhu, Y. Y. Zhao, X. Yi, L. B. Zhu, F. Ge, X. Z. Mou, L. Chen, L. Sun and K. Yang, *Nanoscale*, 2018, **10**, 5114–5123.
72 M. Palmai, A. Petho, L. N. Nagy, S. Klebert, Z. May, J. Mihaly, A. Wacha, K. Jemnitz, Z. Veres, I. Horvath, K. Szigeti, D. Mathe and Z. Varga, *J. Colloid Interface Sci.*, 2017, **498**, 298–305.
73 S. Q. Chen, Q. Y. Jia, X. L. Zheng, Y. M. Wen, W. M. Liu, H. Y. Zhang, J. C. Ge and P. F. Wang, *Sci. China Mater.*, 2018, **61**, 1325–1338.
74 Y. P. Shi, F. Guenneau, X. L. Wang, C. Helary and T. Coradin, *Nanotheranostics*, 2018, **2**, 403–416.
75 M. Y. Zhang, X. J. Liu, Q. Luo, Q. Wang, L. J. Zhao, G. Y. Deng, R. B. Ge, L. Zhang, J. Q. Hu and J. Lu, *Chem. Eng. J.*, 2020, **389**, 124450.
76 Y. W. Hao, L. Wang, B. X. Zhang, D. Li, D. H. Meng, J. J. Shi, H. L. Zhang, Z. Z. Zhang and Y. Zhang, *Int. J. Nanomed.*, 2016, **11**, 1759–1778.
77 Z. F. Ma, X. D. Jia, J. Bai, Y. D. Ruan, C. Wang, J. M. Li, M. C. Zhang and X. Jiang, *Adv. Funct. Mater.*, 2017, **27**, 1604258.
78 J. Z. Liu, W. Z. Zhang, A. Kumar, X. L. Rong, W. Yang, H. M. Chen, J. Xie and Y. M. Wang, *Bioconjugate Chem. Mater.*, 2020, **31**, 82–92.
79 P. J. An, Z. G. Gao, K. Sun, D. H. Gu, H. S. Wu, C. Q. You, Y. J. Li, K. W. Cheng, Y. Zhang, Z. F. Wang and B. W. Sun, *ACS Appl. Mater. Interfaces*, 2019, **11**, 42988–42997.
80 S. Q. Wang, L. T. Yang, H. Y. Cho, S. T. D. Chueng, H. P. Zhang, Q. Y. Zhang and K. B. Lee, *Biomaterials*, 2019, **224**, 119498.
81 R. G. Wang, M. Y. Zhao, D. Deng, X. Ye, F. Zhang, H. Chen and J. L. Kong, *J. Mater. Chem. B*, 2018, **6**, 4592–4601.
82 C. P. Fu, X. H. Duan, M. H. Cao, S. Q. Jiang, X. H. Ban, N. Guo, F. Zhang, J. J. Mao, T. Huyan, J. Shen and L. M. Zhang, *Adv. Healthcare Mater.*, 2019, **8**, 1900047.
83 A. Z. Abbasi, C. R. Gordijo, M. A. Amini, A. Maeda, A. M. Rauth, R. S. DaCosta and X. Y. Wu, *Cancer Res.*, 2016, **76**, 6643–6656.
84 D. P. Sun, J. Lu, Y. W. Zhong, Y. Y. Yu, Y. Wang, B. B. Zhang and Z. G. Chen, *Biosens. Bioelectron.*, 2016, **75**, 301–307.
85 L. Wang, M. Y. Niu, C. X. Zheng, H. J. Zhao, X. X. Niu, L. Li, Y. J. Hu, Y. J. Zhang, J. J. Shi and Z. Z. Zhang, *Adv. Healthcare Mater.*, 2018, **7**, 1800819.
86 Y. Yang, C. Wang, C. Tian, H. L. Guo, Y. H. Shen and M. Z. Zhu, *J. Mater. Chem. B*, 2018, **6**, 6848–6857.
87 F. Gong, J. W. Chen, X. Han, J. Y. Zhao, M. Y. Wang, L. Z. Feng, Y. G. Li, Z. Liu and L. Cheng, *J. Mater. Chem. B*, 2018, **6**, 2250–2257.
88 H. Q. Liu, X. L. Yu, B. Cai, S. J. You, Z. B. He, Q. Q. Huang, L. Rao, S. S. Li, C. Liu, W. W. Sun, W. Liu, S. S. Guo and X. Z. Zhao, *Appl. Phys. Lett.*, 2015, **106**, 093703.
89 S. N. Guan, W. Z. Li, J. R. Ma, Y. Y. Lei, Y. S. Zhu, Q. F. Huang and X. M. Dou, *J. Ind. Eng. Chem.*, 2018, **66**, 126–140.
90 B. B. Ding, P. Zheng, P. A. Ma and J. Lin, *Adv. Mater.*, 2020, **32**, 1905823.
91 X. X. Cai, Q. X. Zhu, Y. Zeng, Q. Zeng, X. L. Chen and Y. H. Zhan, *Int. J. Nanomed.*, 2019, **14**, 8321–8344.

92 B. Liu, F. Hu, J. F. Zhang, C. L. Wang and L. L. Li, *Angew. Chem., Int. Ed.*, 2019, **58**, 8804–8808.
93 J. R. Wu, G. R. Williams, S. W. Niu, Y. B. Yang, Y. Li, X. J. Zhang and L. M. Zhu, *Theranostics*, 2020, **10**, 841–855.
94 B. Jiang, L. Yan, J. L. Zhang, M. Zhou, G. Z. Shi, X. Y. Tian, K. L. Fan, C. Y. Hao and X. Y. Yan, *ACS Appl. Mater. Interfaces*, 2019, **11**, 9747–9755.
95 C. C. Chu, M. Su, J. Zhu, D. S. Li, H. W. Cheng, X. Y. Chen and G. Liu, *Theranostics*, 2019, **9**, 3134–3149.
96 C. Xu, Y. L. Wang, C. Y. Zhang, Y. W. Jia, Y. J. Luo and X. Y. Gao, *Nanoscale*, 2017, **9**, 4620–4628.
97 L. Zhang, Q. Chen, X. W. Zou, J. W. Chen, L. Z. Hu, Z. L. Dong, J. H. Zhou, Y. G. Chen, Z. Liu and L. Cheng, *J. Mater. Chem. B*, 2019, **7**, 5170–5181.
98 J. W. Chen, Q. Chen, C. Liang, Z. J. Yang, L. Zhang, X. Yi, Z. L. Dong, Y. Chao, Y. G. Chen and Z. Liu, *Nanoscale*, 2017, **9**, 14826–14835.
99 W. Zhu, L. Zhang, Z. Yang, P. Liu, J. Wang, J. G. Cao, A. Shen and Z. S. Xu, *Chem. Eng. J.*, 2019, **358**, 969–979.
100 T. S. Lin, X. Z. Zhao, S. Zhao, H. Yu, W. M. Cao, W. Chen, H. Wei and H. Q. Guo, *Theranostics*, 2018, **8**, 990–1004.
101 B. Xiao, X. X. Zhou, H. X. Xu, B. H. Wu, D. Hu, H. J. Hu, K. Y. Pu, Z. X. Zhou, X. R. Liu, J. B. Tang and Y. Q. Shen, *ACS Nano*, 2018, **12**, 12682–12691.
102 A. Sahu, I. Kwon and G Tae, *Biomaterials*, 2020, **228**, 119578.
103 Q. Chen, L. Z. Feng, J. J. Liu, W. W. Zhu, Z. L. Dong, Y. F. Wu and Z. Liu, *Adv. Mater.*, 2016, **28**, 7129–7136.
104 F. L. Gao, J. Wu, H. Q. Gao, X. Y. Hu, L. H. Liu, A. C. Midgley, Q. Q. Liu, Z. Y. Sun, Y. J. Liu, D. Ding, Y. M. Wang, D. L. Kong and X. L. Huang, *Biomaterials*, 2020, **230**, 119635.
105 T. Nonoyama, T. Kinoshita, M. Higuchi, K. Nagata, M. Tanaka, K. Sato and K. Kato, *J. Am. Chem. Soc.*, 2012, **134**, 8841–8847.
106 W. J. Lee, J. M. Lee, S. T. Kochuveedu, T. H. Han, H. Y. Jeong, M. Park, J. M. Yun, J. Kwon, K. No, D. H. Kim and S. O. Kim, *ACS Nano*, 2012, **6**, 935–943.
107 L. R. Zhao, C. H. Fu, L. F. Tan, T. Li, H. S. Zhong and X. W. Meng, *Nanoscale*, 2020, **12**, 2855–2874.
108 X. B. Zhao, Y. D. Qiu, Y. L. Miao, Z. Y. Liu, W. J. Yang and H. W. Hou, *ACS Appl. Nano Mater.*, 2018, **1**, 2621–2631.
109 X. H. Zhu, R. Tang, S. G. Wang, X. Y. Chen, J. J. Hu, C. Y. Lei, Y. Huang, H. H. Wang, Z. Nie and S. Z. Yao, *ACS Nano*, 2020, **14**, 2172–2182.
110 C. W. Lee, S. B. Yoon, S. M. Bak, J. Han, K. C. Roh and K. B. Kim, *J. Mater. Chem. A*, 2014, **2**, 3641–3647.
111 Y. Chen, H. R. Chen, S. J. Zhang, F. Chen, S. K. Sun, Q. J. He, M. Ma, X. Wang, H. X. Wu, L. X. Zhang, L. L. Zhang and J. L. Shi, *Biomaterials*, 2012, **33**, 2388–2398.
112 Y. D. Liu, J. Goebl and Y. D. Yin, *Chem. Soc. Rev.*, 2013, **42**, 2610–2653.
113 W. Li, J. Liu and D. Y. Zhao, *Nat. Rev. Mater.*, 2016, **1**, 16023.
114 N. D. Petkovich and A. Stein, *Chem. Soc. Rev.*, 2013, **42**, 3721–3739.
115 D. G. He, X. X. He, K. M. Wang, X. Yang, X. X. Yang, X. C. Li and Z. Zou, *Chem. Commun.*, 2014, **50**, 11049–11052.
116 J. L. Chen, L. Li, S. Wang, X. Y. Sun, L. Xiao, J. S. Ren, B. Di and N. Gu, *J. Mater. Chem. B*, 2017, **5**, 5336–5344.
117 D. G. He, X. X. He, K. M. Wang, X. Yang, X. X. Yang, Z. Zou and X. C. Li, *Chem. Commun.*, 2015, **51**, 776–779.
118 D. G. He, L. Hai, X. He, Y. Xue and H. W. Li, *Adv. Funct. Mater.*, 2017, **27**, 1704089.
119 L. S. Lin, J. B. Song, L. Song, K. M. Ke, Y. J. Liu, Z. J. Zhou, Z. Y. Shen, J. Li, Z. Yang, W. Tang, G. Niu, H. H. Yang and X. Y. Chen, *Angew. Chem., Int. Ed.*, 2018, **57**, 4902–4906.
120 Y. Y. Zhang, F. Lv, Y. R. Cheng, Z. P. Yuan, F. Yang, C. H. Liu, Y. Cao, K. Zhang, H. T. Lu, S. Zada, S. J. Guo, H. F. Dong and X. J. Zhang, *Adv. Healthcare Mater.*, 2020, **9**, 1901528.
121 G. B. Yang, L. G. Xu, Y. Chao, J. Xu, X. Q. Sun, Y. F. Wu, R. Peng and Z. Liu, *Nat. Commun.*, 2017, **8**, 902.
122 H. J. Wang, D. H. Bremner, K. H. Wu, X. R. Gong, Q. Fan, X. T. Xie, H. M. Zhang, J. Z. Wu and L. M. Zhu, *Chem. Eng. J.*, 2020, **382**, 122848.
123 T. T. Zhang, C. H. Xu, W. Zhao, Y. Gu, X. L. Li, J. J. Xu and H. Y. Chen, *Chem. Sci.*, 2018, **9**, 6749–6757.
124 Y. R. Cheng, F. Yang, K. Zhang, Y. Y. Zhang, Y. Cao, C. H. Liu, H. T. Lu, H. F. Dong and X. J. Zhang, *Adv. Funct. Mater.*, 2019, **29**, 1903850.
125 K. Kai, Y. Yoshida, H. Kageyama, G. Saito, T. Ishigaki, Y. Furukawa and J. Kawamata, *J. Am. Chem. Soc.*, 2008, **130**, 15938–15943.
126 X. N. Jing, Y. Z. Xu, D. M. Liu, Y. S. Wu, N. Zhou, D. Q. Wang, K. Yan and L. J. Meng, *Nanoscale*, 2019, **11**, 15508–15518.
127 Q. Wu, G. Chen, K. K. Gong, J. Wang, X. X. Ge, X. Q. Liu, S. J. Guo and F. Wang, *Matter*, 2019, **1**, 496–512.
128 S. C. Zhang, Q. Z. Li, N. Yang, Y. H. Shi, W. Ge, W. J. Wang, W. Huang, X. J. Song and X. C. Dong, *Adv. Funct. Mater.*, 2019, **29**, 1906805.
129 W. T. Zhang, S. H. Li, X. N. Liu, C. Y. Yang, N. Hu, L. N. Dou, B. X. Zhao, Q. Y. Zhang, Y. R. Suo and J. L. Wang, *Adv. Funct. Mater.*, 2018, **28**, 1706375.
130 Y. H. Sun, H. D. Chen, G. F. Liu, L. N. Ma and Z. X. Wang, *J. Mater. Chem. B*, 2019, **7**, 7152–7161.
131 W. Liu, K. X. Zhang, L. Y. Zhuang, J. J. Liu, W. Zeng, J. J. Shi and Z. Z. Zhang, *Colloids Surf., B*, 2019, **184**, 110536.
132 Y. D. Wang, S. Z. Song, T. Lu, Y. Cheng, Y. L. Song, S. Y. Wang, F. P. Tan, J. Li and N. Li, *Biomaterials*, 2019, **220**, 119405.
133 Q. Q. Sun, H. T. Bi, Z. Wang, C. X. Li, C. Wang, J. T. Xu, D. Yang, F. He, S. L. Gai and P. P. Yang, *ACS Appl. Mater. Interfaces*, 2019, **11**, 36347–36358.
134 Y. S. Feng, D. D. Ding, W. J. Sun, Y. W. Qiu, L. Luo, T. H. Shi, S. S. Meng, X. Y. Chen and H. M. Chen, *ACS Appl. Mater. Interfaces*, 2019, **11**, 37461–37470.

135 X. N. Jing, Z. Zhi, N. Zhang, H. H. Song, Y. Z. Xu, G. Q. Zhou, D. Q. Wang, Y. P. Shao and L. J. Meng, *Chem. Eng. J.*, 2020, **385**, 123893.
136 D. Zhang, Z. J. Ye, L. Wei, H. B. Luo and L. H. Xiao, *ACS Appl. Mater. Interfaces*, 2019, **11**, 39594–39602.
137 Y. Z. Liu, J. Jing, F. Jia, S. Su, Y. Tian, N. Gao, C. L. Yang, R. B. Zhang, W. Z. Wang and X. L. Zhang, *ACS Appl. Mater. Interfaces*, 2020, **12**, 6966–6977.
138 J. B. Pan, Y. Q. Wang, H. Y. Pan, C. Zhang, X. G. Zhang, Y. Y. Fu, X. J. Zhang, C. S. Yu, S. K. Sun and X. P. Yan, *Adv. Funct. Mater.*, 2017, **27**, 1603440.
139 Q. Lu, D. Ericson, Y. Song, C. Z. Zhu and R. F. Ye, *ACS Appl. Mater. Interfaces*, 2017, **9**, 23325–23332.
140 Z. M. He, Y. Xiao, J. R. Zhang, P. H. Zhang and J. J. Zhu, *Chem. Commun.*, 2018, **54**, 2962–2965.
141 X. T. Tian, P. P. Cao, H. Zhang, Y. H. Li and X. B. Yin, *Chem. Commun.*, 2019, **55**, 6241–6244.
142 L. Chudal, N. K. Pandey, J. Phan, O. Johnson, X. Y. Li and W. Chen, *Mater. Sci. Eng., C*, 2019, **104**, 109979.
143 K. F. Xu, H. R. Jia, Y. X. Zhu, X. Y. Liu, G. Gao, Y. H. Li and F. G. Wu, *ACS Biomater.Sci. Eng.*, 2019, **5**, 6072–6081.
144 H. H. Fan, H. R. Bai, Q. Liu, H. Xing, X. B. Zhang and W. H. Tan, *Anal. Chem.*, 2019, **91**, 13143–13151.
145 T. X. Gu, L. Cheng, F. Gong, J. Xu, X. Li, G. R. Han and Z. Liu, *ACS Appl. Mater. Interfaces*, 2018, **10**, 15494–15503.
146 H. J. Zhang, W. W. Zeng, C. Pan, L. W. Feng, M. T. Ou, X. W. Zeng, X. Liang, M. Y. Wu, X. Y. Ji and L. Mei, *Adv. Funct. Mater.*, 2019, **29**, 1903791.
147 C. R. Gordijo, A. Z. Abbasi, M. A. Amini, H. Y. Lip, A. Maeda, P. Cai, P. J. O'Brien, R. S. DaCosta, A. M. Rauth and X. Y. Wu, *Adv. Funct. Mater.*, 2015, **25**, 1858–1872.
148 Y. Liu, Y. P. Zhang, X. M. Li, X. F. Gao, X. Y. Niu, W. Wang, Q. Wu and Z. Yuan, *Nanoscale*, 2019, **11**, 10429–10438.
149 R. J. Liang, L. L. Liu, H. M. He, Z. K. Chen, Z. Q. Han, Z. Y. Luo, Z. H. Wu, M. B. Zheng, Y. F. Ma and L. T. Cai, *Biomaterials*, 2018, **177**, 149–160.
150 D. D. Fu, X. G. Ding, J. Wu, C. Y. Li, Q. B. Wang and J. Jiang, *Part. Part. Syst. Charact.*, 2018, **35**, 1800078.
151 D. W. Zeng, L. Wang, L. Tian, S. L. Zhao, X. F. Zhang and H. Y. Li, *Drug Delivery*, 2019, **26**, 661–672.
152 J. Wen, Y. H. Lv, Y. Q. Xu, P. F. Zhang, H. J. Li, X. X. Chen, X. L. Li, L. K. Zhang, F. Y. Liu, W. X. Zeng and S. G. Sun, *Acta Biomater.*, 2019, **83**, 359–371.
153 G. Linden, L. Zhang, F. Pieck, U. Linne, D. Kosenkov, R. Tonner and O. Vazquez, *Angew. Chem., Int. Ed.*, 2019, **58**, 12868–12873.
154 Y. Zhang, F. M. Wang, C. Q. Liu, Z. Z. Wang, L. H. Kang, Y. Y. Huang, K. Dong, J. S. Ren and X. G. Qu, *ACS Nano*, 2018, **12**, 651–661.
155 S. S. Lucky, K. C. Soo and Y. Zhang, *Chem. Rev.*, 2015, **115**, 1990–2042.
156 J. P. Celli, B. Q. Spring, I. Rizvi, C. L. Evans, K. S. Samkoe, S. Verma, B. W. Pogue and T. Hasan, *Chem. Rev.*, 2010, **110**, 2795–2838.
157 L. Huang, Z. J. Li, Y. Zhao, J. Y. Yang, Y. C. Yang, A. I. Pendharkar, Y. W. Zhang, S. Kelmar, L. Y. Chen, W. T. Wu, J. Z. Zhao and G. Han, *Adv. Mater.*, 2017, **29**, 1604789.
158 R. Vankayala and K. C. Hwang, *Adv. Mater.*, 2018, **30**, 1706320.
159 S. L. Gai, G. X. Yang, P. P. Yang, F. He, J. Lin, D. Y. Jin and B. G. Xing, *Nano Today*, 2018, **19**, 146–187.
160 Q. Y. Jia, J. C. Ge, W. M. Liu, X. L. Zheng, S. Q. Chen, Y. M. Wen, H. Y. Zhang and P. F. Wang, *Adv. Mater.*, 2018, **30**, 1706090.
161 M. N. Wang, J. Z. Zhao, L. S. Zhang, F. Wei, Y. Lian, Y. F. Wu, Z. J. Gong, S. S. Zhang, J. D. Zhou, K. Cao, X. Y. Li, W. Xiong, G. Y. Li, Z. Y. Zeng and C. Guo, *J. Cancer*, 2017, **8**, 761–773.
162 J. Kim, H. R. Cho, H. Jeon, D. Kim, C. Song, N. Lee, S. H. Choi and T. Hyeon, *J. Am. Chem. Soc.*, 2017, **139**, 10992–10995.
163 J. M. Chen, T. J. Fan, Z. J. Xie, Q. Q. Zeng, P. Xue, T. T. Zheng, Y. Chen, X. L. Luo and H. Zhang, *Biomaterials*, 2020, **237**, 119827.
164 E. Ju, K. Dong, Z. W. Chen, Z. Liu, C. Q. Liu, Y. Y. Huang, Z. Z. Wang, F. Pu, J. S. Ren and X. G. Qu, *Angew. Chem., Int. Ed.*, 2016, **55**, 11467–11471.
165 W. Zhang, J. Lu, X. N. Gao, P. Li, W. Zhang, Y. Ma, H. Wang and B. Tang, *Angew. Chem., Int. Ed.*, 2018, **57**, 4891–4896.
166 C. D. Ji, Q. Gao, X. H. Dong, W. Y. Yin, Z. J. Gu, Z. H. Gan, Y. L. Zhao and M. Z. Yin, *Angew. Chem., Int. Ed.*, 2018, **57**, 11384–11388.
167 P. Huang, J. Lin, X. S. Wang, Z. Wang, C. L. Zhang, M. He, K. Wang, F. Chen, Z. M. Li, G. X. Shen, D. X. Cui and X. Y. Chen, *Adv. Mater.*, 2012, **24**, 5104–5110.
168 G. B. Yang, L. G. Xu, J. Xu, R. Zhang, G. S. Song, Y. Chao, L. Z. Feng, F. X. Han, Z. L. Dong, B. Li and Z. Liu, *Nano Lett.*, 2018, **18**, 2475–2484.
169 H. Min, J. Wang, Y. Q. Qi, Y. L. Zhang, X. X. Han, Y. Xu, J. C. Xu, Y. Li, L. Chen, K. M. Cheng, G. N. Liu, N. Yang, Y. Y. Li and G. J. Nie, *Adv. Mater.*, 2019, **31**, 1808200.
170 H. H. Fan, G. B. Yan, Z. L. Zhao, X. X. Hu, W. H. Zhang, H. Liu, X. Y. Fu, T. Fu, X. B. Zhang and W. H. Tan, *Angew. Chem., Int. Ed.*, 2016, **55**, 5477–5482.
171 H. T. Bi, Y. L. Dai, P. P. Yang, J. T. Xu, D. Yang, S. L. Gai, F. He, G. H. An, C. N. Zhong and J. Lin, *Chem. Eng. J.*, 2019, **356**, 543–553.
172 B. J. Ma, S. Wang, F. Liu, S. Zhang, J. Z. Duan, Z. Li, Y. Kong, Y. H. Sang, H. Liu, W. B. Bu and L. L. Li, *J. Am. Chem. Soc.*, 2019, **141**, 849–857.
173 K. Sato, S. Shimizu, K. Awaji, O. Hitomi and J. I. Anzai, *J. Colloid Interface Sci.*, 2018, **510**, 302–307.
174 W. W. Zhu, Z. L. Dong, T. T. Fu, J. J. Liu, Q. Chen, Y. G. Li, R. Zhu, L. G. Xu and Z. Liu, *Adv. Funct. Mater.*, 2016, **26**, 5490–5498.
175 C. Zhang, W. H. Chen, L. H. Liu, W. X. Qiu, W. Y. Yu and X. Z. Zhang, *Adv. Funct. Mater.*, 2017, **27**, 1700626.
176 H. J. Zhu, J. C. Li, X. Y. Qi, P. Chen and K. Y. Pu, *Nano Lett.*, 2018, **18**, 586–594.

177 J. T. Liu, P. Du, T. R. Liu, B. J. C. Wong, W. P. Wang, H. X. Ju and J. P. Lei, *Biomaterials*, 2019, **192**, 179–188.
178 S. Kapri and S. Bhattacharyya, *Chem. Sci.*, 2018, **9**, 8982–8989.
179 W. H. Chen, J. H. Liu, Y. Wang, C. H. Jiang, B. Yu, Z. Sun and L. H. Lu, *Angew. Chem., Int. Ed.*, 2019, **58**, 6290–6294.
180 M. Cheng, Y. X. Cui, J. Wang, J. Zhang, L. N. Zhu and D. M. Kong, *ACS Appl. Mater. Interfaces*, 2019, **11**, 13158–13167.
181 C. C. Chu, H. R. Lin, H. Liu, X. Y. Wang, J. Q. Wang, P. F. Zhang, H. Y. Gao, C. Huang, Y. Zeng, Y. Z. Tan, G. Liu and X. Y. Chen, *Adv. Mater.*, 2017, **29**, 1605928.
182 H. X. Li, X. Yan, D. S. Kong, R. Jin, C. Y. Sun, D. Du, Y. H. Lin and G. Y. Lu, *Nanoscale Horiz.*, 2020, **5**, 218–234.
183 N. H. Ly and S. W. Joo, *J. Mater. Chem. B*, 2020, **8**, 186–198.
184 L. C. Chen, S. F. Zhou, L. C. Su and J. B. Song, *ACS Nano*, 2019, **13**, 10887–10917.
185 S. M. Li, L. F. Tan and X. W. Meng, *Adv. Funct. Mater.*, 2020, **30**, 1908924.
186 S. Shaikh, F. U. Rehman, T. Y. Du, H. Jiang, L. H. Yin, X. M. Wang and R. J. Chai, *ACS Appl. Mater. Interfaces*, 2018, **10**, 26056–26063.
187 T. Kim, H. J. Jang, S. Kim, J. H. Lee, S. Y. Kim, N. L. Jeon, J. M. Song and D. H. Min, *Langmuir*, 2018, **34**, 173–178.
188 J. M. Xiao, G. L. Zhang, R. Xue, H. Chen, H. J. Wang, G. Tian, B. Wang, C. Yang, G. Bai, Z. Y. Zhang, H. Y. Yang, K. Zhong, D. H. Zou and Z. Y. Wu, *Biomaterials*, 2019, **216**, 119254.
189 T. He, H. Xu, Y. F. Zhang, S. J. Yi, R. Cui, S. J. Xing, C. L. Wei, J. Lin and P. Huang, *Theranostics*, 2020, **10**, 1544–1554.
190 X. Hu, X. D. Liu, X. D. Zhang, H. Y. Cao and Y. M. Huang, *Sens. Actuators, B*, 2019, **286**, 476–482.
191 Z. L. Song, X. Dai, M. R. Li, H. Teng, Z. Song, D. X. Xie and X. L. Luo, *Microchim. Acta*, 2018, **185**, 485.
192 R. X. Song, M. Zhang, Y. Y. Liu, Z. W. Cui, H. Zhang, Z. M. Tang, X. Y. Chen, H. H. Wu, Z. W. Yao, M. Y. He and W. B. Bu, *Biomaterials*, 2018, **175**, 123–133.
193 L. H. Jin, J. H. Liu, Y. Tang, L. Q. Cao, T. Q. Zhang, Q. H. Yuan, Y. H. Wang and H. J. Zhang, *ACS Appl. Mater. Interfaces*, 2017, **9**, 41648–41658.
194 M. Zhang, L. Xing, H. T. Ke, Y. J. He, P. F. Cui, Y. Zhu, G. Jiang, J. B. Qiao, N. Lu, H. B. Chen and H. L. Jiang, *ACS Appl. Mater. Interfaces*, 2017, **9**, 11337–11344.
195 J. R. Peng, M. L. Dong, B. Ran, W. T. Li, Y. Hao, Q. Yang, L. W. Tan, K. Shi and Z. Y. Qian, *ACS Appl. Mater. Interfaces*, 2017, **9**, 13875–13886.
196 Y. Chen, D. L. Ye, M. Y. Wu, H. R. Chen, L. L. Zhang, J. L. Shi and L. Z. Wang, *Adv. Mater.*, 2014, **26**, 7019–7026.
197 Q. Q. Sun, F. He, C. Q. Sun, X. X. Wang, C. X. Li, J. T. Xu, D. Yang, H. T. Bi, S. L. Gai and P. P. Yang, *ACS Appl. Mater. Interfaces*, 2018, **10**, 33901–33912.
198 W. B. Shi, B. Song, W. J. Shi, X. D. Qin, Z. W. Liu, M. Q. Tan, L. Wang, F. L. Song and J. L. Yuan, *ACS Appl. Mater. Interfaces*, 2018, **10**, 27681–27691.
199 Z. L. Zhao, H. H. Fan, G. F. Zhou, H. R. Bai, H. Liang, R. W. Wang, X. B. Zhang and W. H. Tan, *J. Am. Chem. Soc.*, 2014, **136**, 11220–11223.
200 M. Banobre-Lopez, L. Garcia-Hevia, M. F. Cerqueira, F. Rivadulla and J. Gallo, *Chem. – Eur. J.*, 2018, **24**, 1295–1303.
201 J. L. Sun, F. Liu, W. Q. Yu, Q. Y. Jiang, J. L. Hu, Y. H. Liu, F. Wang and X. Q. Liu, *Nanoscale*, 2019, **11**, 5014–5020.
202 V. Revuri, K. Cherukula, M. Nafiujjaman, K. J. Cho, I. K. Park and Y. K. Lee, *ACS Appl. Nano Mater.*, 2018, **1**, 662–674.
203 Y. Wu, D. Li, F. Zhou, H. Liang, Y. Liu, W. J. Hou, Q. Yuan, X. B. Zhang and W. H. Tan, *Chem. Sci.*, 2018, **9**, 5427–5434.
204 L. L. Feng, R. Xie, C. Q. Wang, S. L. Gai, F. He, D. Yang, P. P. Yang and J. Lin, *ACS Nano*, 2018, **12**, 11000–11012.
205 S. N. Li, L. Y. Zhang, X. J. Chen, T. T. Wang, Y. Zhao, L. Li and C. G. Wang, *ACS Appl. Mater. Interfaces*, 2018, **10**, 24137–24148.
206 L. T. Meng, Y. L. Cheng, X. N. Tong, S. J. Gan, Y. W. Ding, Y. Zhang, C. Wang, L. Xu, Y. S. Zhu, J. H. Wu, Y. Q. Hu and A. Yuan, *ACS Nano*, 2018, **12**, 8308–8322.
207 X. D. Lin, Y. Fang, Z. H. Tao, X. Gao, T. L. Wang, M. Y. Zhao, S. Wang and Y. Q. Liu, *ACS Appl. Mater. Interfaces*, 2019, **11**, 25043–25053.
208 V. Revuri, K. Cherukula, M. Nafiujjaman, V. Vijayan, Y. Y. Jeong, I. K. Park and Y. K. Lee, *ACS Appl. Mater. Interfaces*, 2019, **11**, 19782–19792.
209 F. Chen, M. Bai, K. Cao, Y. Zhao, J. Wei and Y. X. Zhao, *Adv. Funct. Mater.*, 2017, **27**, 1702748.
210 J. P. Sheng, X. X. Jiang, L. Q. Wang, M. H. Yang and Y. N. Liu, *Anal. Chem.*, 2018, **90**, 2926–2932.
211 L. Han, S. G. Liu, J. Y. Liang, N. B. Li and H. Q. Luo, *Sens. Actuators, B*, 2019, **288**, 195–201.
212 C. A. Choi, B. Ryplida, I. In and S. Y. Park, *Eur. J. Pharm. Sci.*, 2019, **134**, 256–265.
213 D. D. Yuan, L. R. Ding, Z. M. Sun and X. M. Li, *Sci. Rep.*, 2018, **8**, 1747.
214 Y. G. Wang, G. H. Zhao, H. Wang, W. Cao, B. Du and Q. Wei, *Biosens. Bioelectron.*, 2018, **106**, 179–185.
215 P. Zhao, Y. H. Zhu, X. L. Yang, J. H. Shen, X. Jiang, J. Zong and C. Z. Li, *Dalton Trans.*, 2014, **43**, 451–457.
216 L. Zhao, X. Q. Ge, H. J. Zhao, L. Y. Shi, J. A. Capobianco, D. Y. Jin and L. N. Sun, *ACS Appl. Nano Mater.*, 2018, **1**, 1648–1656.
217 X. Yang, D. G. He, X. X. He, K. M. Wang, Z. Zou, X. C. Li, H. Shi, J. R. Luo and X. X. Yang, *Part. Part. Syst. Charact.*, 2015, **32**, 205–212.
218 Z. Z. Wang, Y. Zhang, Z. Liu, K. Dong, C. Q. Liu, X. Ran, F. Pu, E. Ju, J. S. Ren and X. G. Qu, *Nanoscale*, 2017, **9**, 14236–14247.
219 X. L. Hu, Q. Y. Cai, J. Gao, R. A. Field, G. R. Chen, N. Y. Jia, Y. Zang, J. Li and X. P. He, *ACS Appl. Mater. Interfaces*, 2019, **11**, 22181–22187.
220 Z. Zhang and Y. H. Ji, *Chin. J. Chem. Eng.*, 2020, **28**, 1405–1414.

221 Y. Yao, N. Li, X. Zhang, J. O. Machuki, D. Z. Yang, Y. Y. Yu, J. J. Li, D. Q. Tang, J. W. Tian and F. L. Gao, *ACS Appl. Mater. Interfaces*, 2019, **11**, 13991–14003.
222 Q. Y. Tang, Z. J. Cheng, N. Yang, Q. Z. Li, P. Wang, D. P. Chen, W. J. Wang, X. J. Song and X. C. Dong, *Biomaterials*, 2019, **205**, 1–10.
223 Z. Zhang and Y. H. Ji, *Ind. Eng. Chem. Res.*, 2019, **58**, 2991–2999.
224 C. Liu, D. P. Wang, Y. Zhan, L. Y. Yan, Q. Lu, M. Y. Z. Chang, J. W. Luo, L. D. Wang, D. Du, Y. H. Lin, J. Xia and Y. Wu, *ACS Appl. Mater. Interfaces*, 2018, **10**, 44231–44239.
225 J. J. Liu, Q. Chen, W. W. Zhu, X. Yi, Y. Yang, Z. L. Dong and Z. Liu, *Adv. Funct. Mater.*, 2017, **27**, 1605926.
226 L. L. Tian, Q. Chen, X. Yi, J. W. Chen, C. Liang, Y. Chao, K. Yang and Z. Liu, *Small*, 2017, **13**, 1700640.
227 Z. Z. Wang, Y. Zhang, E. G. Ju, Z. Liu, F. F. Cao, Z. W. Chen, J. S. Ren and X. G. Qu, *Nat. Commun.*, 2018, **9**, 3334.
228 Y. Cao, X. D. Meng, D. D. Wang, K. Zhang, W. H. Dai, H. F. Dong and X. J. Zhang, *ACS Appl. Mater. Interfaces*, 2018, **10**, 17732–17741.
229 G. B. Yang, R. Zhang, C. Liang, H. Zhao, X. Yi, S. D. Shen, K. Yang, L. Cheng and Z. Liu, *Small*, 2018, **14**, 1702664.
230 M. L. Shi, S. Wang, S. H. Zheng, P. F. Hou, L. N. Dong, M. J. He, C. Wu, X. L. Zhang, F. M. Zuo, K. Xu and J. J. Li, *Colloids Surf., B*, 2020, **185**, 110625.
231 F. Gao, Y. Tang, W. L. Liu, M. Z. Zou, C. Huang, C. J. Liu and X. Z. Zhang, *Adv. Mater.*, 2019, **31**, 1904639.
232 G. Delaney, S. Jacob, C. Featherstone and M. Barton, *Cancer*, 2005, **104**, 1129–1137.
233 W. Pan, B. J. Cui, P. Gao, Y. G. Ge, N. Li and B. Tang, *Chem. Commun.*, 2020, **56**, 547–550.
234 H. Yang, H. P. He, Z. R. Tong, H. B. Xia, Z. W. Mao and C. Y. Gao, *J. Colloid Interface Sci.*, 2020, **565**, 186–196.
235 Z. Liu, S. J. Zhang, H. Lin, M. L. Zhao, H. L. Yao, L. L. Zhang, W. J. Peng and Y. Chen, *Biomaterials*, 2018, **155**, 54–63.
236 W. Tang, W. P. Fan, W. Z. Zhang, Z. Yang, L. Li, Z. T. Wang, Y. L. Chiang, Y. J. Liu, L. M. Deng, L. C. He, Z. Y. Shen, O. Jacobson, M. A. Aronova, A. Jin, J. Xie and X. Y. Chen, *Adv. Mater.*, 2019, **31**, 1900401.
237 S. C. Zhang, C. Y. Cao, X. Y. Lv, H. M. Dai, Z. H. Zhong, C. Liang, W. J. Wang, W. Huang, X. J. Song and X. C. Dong, *Chem. Sci.*, 2020, **11**, 1926–1934.
238 B. B. Ding, S. Shao, F. Jiang, P. P. Dang, C. Q. Sun, S. S. Huang, P. A. Ma, D. Y. Jin, A. A. Al Kheraif and J. Lin, *Chem. Mater.*, 2019, **31**, 2651–2660.
239 Y. Y. Zhao, E. W. Xu, X. Q. Yang, Y. Zhang, H. Chen, Y. Wang and M. L. Jin, *Virchows Arch.*, 2020, **477**, 401–408.
240 S. N. Zhou, W. T. Pan, M. X. Pan, Q. Y. Luo, L. Zhang, J. Z. Lin, Y. J. Zhao, X. L. Yan, L. P. Yuan, Y. X. Zhang, D. J. Yang and M. Z. Qiu, *Dig. Dis. Sci.*, DOI: 10.1007/s10620-020-06203-8.
241 S. Y. Guo, D. Sun, D. L. Ni, M. R. Yu, K. Qian, W. Zhang, Y. W. Yang, S. Song, Y. Li, Z. Y. Xi, J. Wang, J. Y. Li, Y. Wei, K. X. Chen, Y. Gan and Z. T. Wang, *Adv. Funct. Mater.*, 2020, **30**, 2000486.
242 M. Yu, X. H. Duan, Y. J. Cai, F. Zhang, S. Q. Jiang, S. S. Han, J. Shen and X. T. Shuai, *Adv. Sci.*, 2019, **6**, 1900037; F. Liu, L. Lin, Y. Zhang, S. Sheng, Y. B. Wang, C. N. Xu, H. Y. Tian and X. S. Chen, *Biomaterials*, 2019, **223**, 119470.